




Integrative analyses reveal *Bna-miR397a*–*BnaLAC2* as a potential modulator of low-temperature adaptability in *Brassica napus* L.

Muhammad Azhar Hussain^{1,†}, Yong Huang^{1,†}, Dan Luo¹, Sundas Saher Mehmood¹, Ali Raza¹ , Liu Duan², Xuekun Zhang³, Yong Cheng¹, Hongtao Cheng¹, Xiling Zou¹, Xiaoyu Ding¹, Liu Zeng¹, Bian Wu⁴, Keming Hu^{2,5,*}  and Yan Lv^{1,*} 

¹Key Laboratory of Biology and Genetic Improvement of Oil Crops, Ministry of Agriculture, Oil Crops Research Institute of the Chinese Academy of Agricultural Sciences (CAAS), Wuhan, China

²State Key Laboratory of Biocatalysis and Enzyme Engineering, School of Life Sciences, Hubei University, Wuhan, China

³Yangtze University, Jingzhou, China

⁴Food Crops Institute, Hubei Academy of Agricultural Sciences, Wuhan, China

⁵Jiangsu Key Laboratory of Crop Genomics and Molecular Breeding/Key Laboratory of Plant Functional Genomics of the Ministry of Education/Jiangsu Key Laboratory of Crop Genetics and Physiology, College of Agriculture, Yangzhou University, Yangzhou, China

Received 11 October 2023;

revised 2 December 2024;

accepted 12 February 2025.

*Correspondence (Tel 86-027-86811837; fax 86-027-86816451; email lyan01@caas.cn (Y.L.); Tel 86-0514-87972136; fax 86-0514-87311374; email hukm@yzu.edu.cn (K.H.))

†These authors contributed equally to this work.

[Correction added on 10 April 2025, after first online publication: The order of the author and affiliation is updated in this version.]

Keywords: *B. napus*, cold stress, *Bna-miR397a*, *BnaLAC2*, lignin, ROS homeostasis.

Summary

Brassica napus L. (*B. napus*) is a major edible oil crop grown around the southern part of China, which often faces cold stress, posing potential damage to vegetative tissues. To sustain growth and reproduction, a detailed understanding of fundamental regulatory processes in *B. napus* against long-term low temperature (LT) stress is necessary for breeders to adjust the level of LT adaption in a given region and is therefore of great economic importance. Till now, studies on microRNAs (miRNAs) in coping with LT adaption in *B. napus* are limited. Here, we performed an in-depth analysis on two *B. napus* varieties with distinct adaptability to LT stress. Through integration of RNA sequencing (RNA-seq) and small RNA-sequencing (sRNA-seq), we identified 106 modules comprising differentially expressed miRNAs and corresponding potential targets based on strong negative correlations between their dynamic expression patterns. Specifically, we demonstrated that *Bna-miR397a* post-transcriptionally regulates a LACCASE (LAC) gene, *BnaLAC2*, to enhance the adaption to LT stresses in *B. napus* by reducing the total lignin remodelling and ROS homeostasis. In addition, the *miR397*–*LAC2* module was also proved to improve freezing tolerance of *Arabidopsis*, indicating a conserved role of *miR397*–*LAC2* in *Cruciferae* plants. Overall, this work provides the first description of a miRNA-mediated-module signature for LT adaption and highlights the prominent role of laccase in future breeding programme of LT tolerant *B. napus*.

Introduction

Brassica napus L. (*B. napus*) is the largest oilseed crop in China. China contributes 20% of the world's *B. napus* production with 7.5 million hectares of planting area, but the self-sufficiency rate of edible oil is still <40%. The double-cropping rice area such as Yangtze River Basin is the main producing area of *B. napus* in China (Wang, 2018). As a winter crop, *B. napus* in this region is often rotated with rice, known as Rice-Rice-*B. napus* triple cropping, which is conducive to promoting the abundance of grain and oil, ecological restoration as well as green and sustainable development (Xiao *et al.*, 2022). At present, there are still more than 6 million hectares of winter fallow fields in the Yangtze River Basin, of which 4.27 million hectares are suitable for the rice-*B. napus* rotation mode, accounting for nearly 80% of the total potential planting area of *B. napus* in China (Liu *et al.*, 2019). One trade-off to this regional potential of land resource is that the continuous delay of the late-rice harvesting period puts the winter *B. napus* (early-maturing *B. napus*) under the test of low temperatures (LTs). During late-fall and winter,

minimum air temperatures in this region can vary from 20 °C to as low as 0 °C (Huang *et al.*, 2020). Normally, exposure to cold (0–15 °C) or freezing (<0 °C) temperature for a long period affects the seed germination ratio, restrict growth and development of seedlings, and reduce yield and quality (Ding and Yang, 2022). Thus, improving LT tolerance of *B. napus* is of major interest given its crucial role in adapting agricultural practice to unfavourable climates.

Plants undergo substantial physiological, biochemical and molecular adaptations to withstand the deleterious impacts associated with LTs, and the ICE (Inducer of CBF Expression)–CBF (C-repeat Binding Factor)–COR (Cold Regulated genes) signalling pathway has been, thus far, the best identified module in plants under cold stress (Yang, 2022). Known as dehydration-responsive element binding (DREB) factors, *CBFs* can be triggered by ICE upon exposure to LTs via an abscisic acid (ABA)-independent pathway (Shi *et al.*, 2018; Thomashow, 2010). *CBFs* then bind directly to the promoter of *COR* genes, subsequently transducing cold signals. Numerous regulators are involved in this pathway, fine-tuning the core elements at diverse

molecular levels, such as cold-responsive protein kinase 1 (CRPK1) (Liu *et al.*, 2017b), open stomatal 1 (OST1) (Ding *et al.*, 2019), calmodulin-binding transcription activator protein 1–5 (CAMTA1–5) (Kidokoro *et al.*, 2017), phytochrome interacting factor 3/4/7 (PIF3/4/7) (Jiang *et al.*, 2017) and brassinazole resistant 1 (BZR1) (Qi *et al.*, 2021).

Apart from ICE–CBF–COR mediated cold signalling pathway, miRNAs have recently attracted considerable attention for their engagements in plant LT adaption (Huo *et al.*, 2022). These small non-coding RNAs, with approximately 21–24 nucleotides in length, often act as guide molecules of the RNA-induced silencing complex (RISC) to degrade target mRNAs, or prevent their translation (Beauclair *et al.*, 2010; Tang and Chu, 2017). Initial work on *Arabidopsis* has revealed differential profiling of LT-induced miRNAs, including *At-miR397* (Sunkar and Zhu, 2004). Subsequent work has corroborated its vital role in cold acclimation: *Arabidopsis* overexpressing *At-miR397a* exhibits enhanced cold hardiness (Dong and Pei, 2014), which was partially due to the accumulated transcripts of *CBF2* and downstream *COR* genes. However, some discrepancy was observed in wheat seedlings since reduced level of *miR397* would also help plants adapt to LT stress, accompanied by up-regulation of *ICE1* (Gupta *et al.*, 2014). One of the conserved targets predicted or confirmed for miR397 in plants are members encoding laccase (LAC) multicopper oxidase. While LACs are known to participate in the biosynthesis of lignin, their precise roles in cold adaption remain elusive (Wang *et al.*, 2014a; Xue *et al.*, 2019).

In rice, functional roles of miRNAs have also been found in response to LT stress. For example, *Osa-miR319a* and *Osa-miR319b* are found to enhance the cold tolerance (4 °C) of seedlings, while *OsPCF5* and *OsPCF8* were identified as the direct target of *miR319s*. Post translational silencing of *OsPCF5* and *OsPCF8* dramatically improves the cold tolerance of transgenic plants, thus confirming the positive role of *miR319-OsPCFs* module in cold tolerance of rice plants (Yang *et al.*, 2013). In *Arabidopsis*, *miR394* has been shown to target *AtLCR* that encodes a putative F-box protein, in response to salinity and drought stress (Song *et al.*, 2013). The positive role of this miRNA-target module in response to LT stress (4 to –11 °C) was also demonstrated in other studies (Song *et al.*, 2016). In addition to enhanced expression of cold-responsive genes, *At-miR394a* OE lines and *Atlcr* mutant also showed a higher survival rate, free proline levels and soluble sugars when compared with corresponding WT plants. In wheat, *tae-miR398* triggers a regulatory loop that might critically affect cold tolerance (Lu *et al.*, 2020). While *tae-miR398* is downregulated and negatively related to its target, *TaCSD1*, as the temperature drops, *tae-miR398* could also be modulated by cold-induced lncRNAs (lncR117, lncR9A and lncR616). These lncRNAs actively interact with *tae-miRNA398*, reducing its effective concentration to cleave *TaCSD1* in a competitive way. Therefore, the accumulated level of *TaCSD1* might boost the ability of plant to scavenge excessive ROS produced by LTs.

Despite numerous studies highlighting the key roles of miRNAs in crops like rice, maize and wheat (Aydinoglu, 2020; Fang *et al.*, 2017; Song *et al.*, 2017), only a few attempts have been made to provide clues on the relevance of these molecules in *B. napus* cold adaptation. Through a sRNA-seq approach, Megha *et al.* (2018) identified 129 DEMs in a spring-type line of *B. napus*, after 48 h-cold treatment (4 °C), of which 104 are

novel miRNAs and 25 are conserved (Megha *et al.*, 2018). However, the precise correlation based on miRNA–mRNA interactions remains to be better understood. Meanwhile, very limited data are available on functionally characterized LT-related genes in *B. napus*, except for classical *CBFs* and *COR* genes (Chen *et al.*, 2011; Dahal *et al.*, 2012; Orvar *et al.*, 2000; Savitch *et al.*, 2005).

We previously evaluated the adaptations of 226 *B. napus* varieties/lines under short-term cold and freezing stress conditions, in which line C18 exhibited excellent cold hardiness, while line C6 was sensitive to LT (Yan *et al.*, 2018). To better understand the complex mechanism of prolonged cold acclimation in *B. napus*, here we conducted a comparative analysis of miRNAome and transcriptome profiles for C18 and C6, with a goal of identifying cold-responsive miRNAs and corresponding target genes, as well as revealing their contributions to cold stress tolerance. By doing so, we have successfully identified the module *Bna-miR397a–BnaLAC2* that helps C18 achieve tolerance to long-term LT conditions via modifying lignin contents of *B. napus*, which thus provides a genetic resource for breeding cold-adaptive *B. napus* varieties by editing *Bna-miR397a* and its target *BnaLAC2*.

Results

Performances of two *B. napus* varieties under LTs

Previously, we investigated the freezing tolerance and cold acclimation responses of 226 *B. napus* lines (Yan *et al.*, 2018, 2019). In these screening studies, *B. napus* line C18 exhibited greater tolerant to freezing temperatures (gradient from –2 °C to –6 °C) during a 3 h treatment compared to a typical cold-sensitive line, C6. These findings suggested that C18 could be a promising candidate for cultivation in the Yangtze River Basin. However, the continuous delay of the late-rice harvesting period exposes *B. napus* to prolonged low temperatures (≥ 2 weeks), which can reduce overwintering rates and yield. Therefore, we investigated the response of C18 to extended cold exposure. As depicted in Figure 1a, cold treatment limited the growth of both C6 and C18, but to differing extents. After 7 days, all true leaves of C6 curled and the third true leaf remained stunted. Conversely, the third true leaf of C18 fully expanded by this time, and the fourth true leaf emerged after 14 days. This contrasted with C6, where the fourth true leaf did not emerge until day 21. Furthermore, C6 began exhibiting chlorosis on its leaves as early as 7 days into the cold treatment, while in C18, chlorosis was only minimally observed after 14 days. This visual difference was reflected at the cellular level: light microscopy revealed more pronounced cold-induced plasmolysis (i.e. shrinkage of parenchyma cells) in C6 compared to C18 after cold treatment (Figure S1a). The proportion of shrunken cells in C6 at 21 DAC was approximately 1.6 times greater than that in C18 (Figure S1b). This cellular damage paralleled declining photosynthetic efficiency in both varieties, though C18 consistently outperformed C6. Specifically, C18 maintained higher chlorophyll content than C6 by 10.4%, 19.6% and 30.7% at 7, 14 and 21 DAC, respectively ($P < 0.05$) (Figure 1b). Similarly, C18 showed marginally higher Fv/Fm values, exceeding C6 by 2.3%, 1.8% and 1.9% at corresponding timepoints (Figure 1c).

To obtain a reliable estimate of LTs tolerance between the two lines, fresh weight (FW) was measured before and after the cold

treatment. Upon the exposure to low temperatures, the FW generally increased in both C18 and C6. However, C18 exhibited significantly greater FW accumulation than the cold-sensitive line C6 after 1 week of cold stress (Figure 1d). The changes in proline content followed a similar pattern to FW, with the significant difference between the two lines becoming evident on day 14 of cold treatment (Figure 1e).

Since an increase in percentage electrolyte leakage (EL) following cold stress is a reliable indicator of membrane injury (Campos *et al.*, 2003), we assessed the EL of both lines during cold exposure (Figure 1f): The EL of C6 seedling increased sharply within 1 day of cold exposure and continued to rise over the subsequent 20 days. While C18 displayed a similar trend, its rate of increase fluctuated: the EL remained gradual from 0 to 7 days, rarely exceeding 28% compared to day 0. Even though EL in C18 eventually increased with prolonged cold exposure, it remained

markedly lower than that observed in C6, particularly during the initial days.

In plants, proline accumulation subjected to LTs appears to be a universal phenomenon (Ding and Yang, 2022). The more tolerant C18 exhibited a steady increase in proline content, while in C6, proline accumulated initially, followed by a slight decrease on days 14 and 21 of cold treatment. These results suggest that C18 exhibits a greater ability to adapt to long-term LT stress.

Integrated analysis of differentially expressed miRNAs (DEMs) and genes (DEGs) induced by LTs

To determine how the two *B. napus* lines differ in their responses to cold stress, we performed a stepwise approach to integrate the miRNA and mRNA sequencing data sets of cold-treated samples.

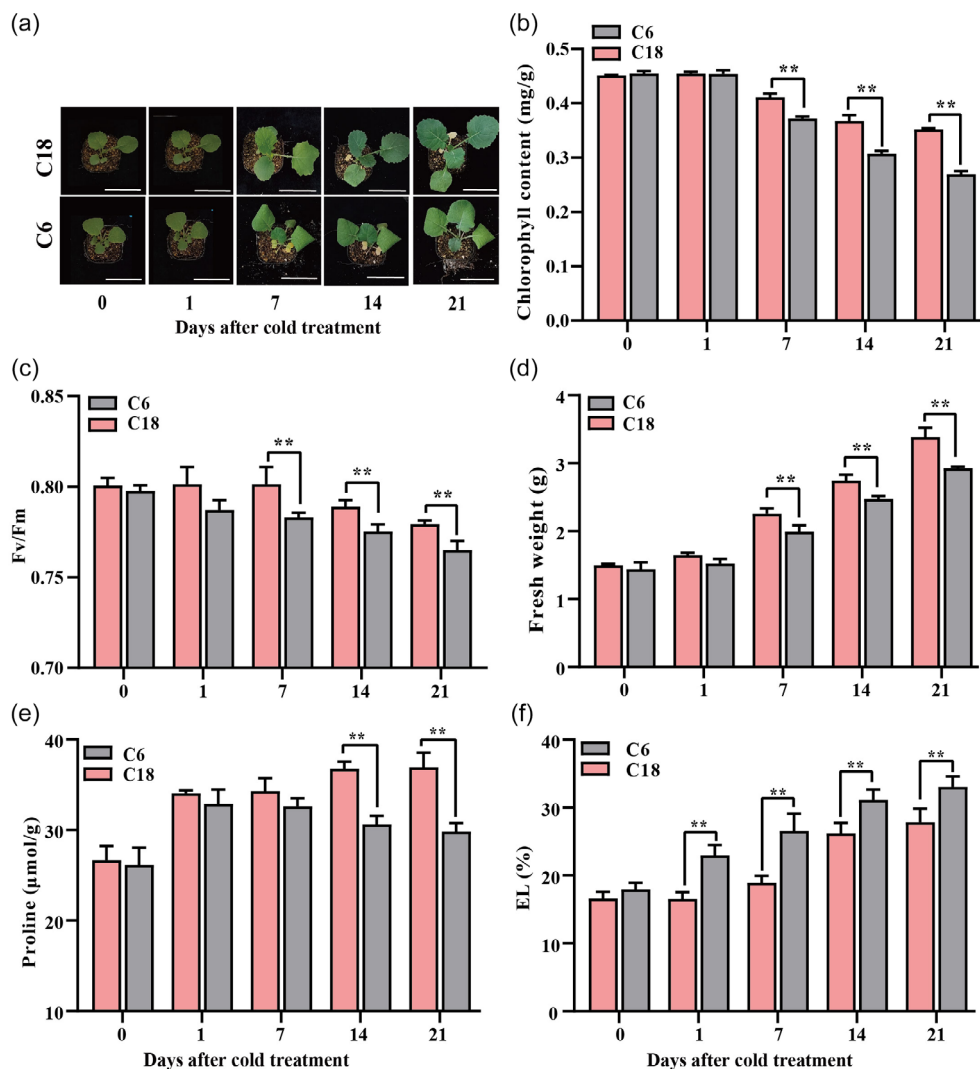


Figure 1 The phenotypic and physiological responses of two *Brassica napus* lines to cold stress. (a) The phenotypes displayed by cold-treated (4–8 °C) *B. napus* lines C18 (left panels, cold-tolerant) and C6 (right panels, cold-sensitive) at the seedling stage. Scale bar = 10 cm. Determination of the physiological parameters, (b) chlorophyll content (mg/g), (c) Fv/Fm, (d) fresh weight (g), (e) proline content (μmol/g) and (f) electrolyte leakage (EL, %). Each data represents the mean (three to six replicates) ± standard deviation of the measurements on the different plants. The asterisks represent a significant difference was detected between C18 and C6 subjected to the same treatment at $P < 0.01$ (**).

DEMs induced by LTs

To characterize miRNAs in *B. napus* upon long-term cold exposure, small RNA (sRNA) libraries were constructed from C18 and C6 leaves following 0, 1, 7, 14 and 21 days of cold treatment and sequenced using Illumina technology. In total, 81 conserved miRNAs, representing 31 miRNA families, exhibited high sequence match to currently known plant mature miRNAs. The length of conserved miRNAs, also referred to as known miRNAs, ranged from 20 to 24 nucleotides (nt), with a predominant length of 21 nt (82.7%) (Figure S2). Meanwhile, 163 miRNAs were classified as novel miRNAs (Table S1). The length of these novel miRNAs ranged from 18 to 25 nt, with 21 nt being the most abundant, followed by 24 nt (Figure S2).

Thirty-five conserved miRNAs and 111 novel miRNAs were differentially expressed ($|\log_2 FC| \geq 1.5$, $P \leq 0.05$) in response to LTs (Figure 2a,b; Table S2). Previously, Megha *et al.* (2018) reported 25 conserved cold-responsive miRNA families in *B. napus* under short-term cold stress, with 80% also identified in our study. This overlap suggests that these miRNAs are functionally conserved in the cold response, reinforcing the reliability of our findings. However, we also identified DEMs not reported by Megha *et al.* (2018), such as *Bna-miR164*, *Bna-miR166*, *Bna-miR169*, *Bna-miR172* and *Bna-miR390*, while we did not detect *Bna-miR398*. A Venn diagram analysis indicated that six and three DEMs were shared across all time points in C6 and C18, respectively (Figure 2a,b). Furthermore, the cold-tolerant variety, C18, exhibited a higher number of DEMs (112) compared to the cold-sensitive variety, C6 (94) (Table S2).

Considerable variations in expression were observed among individual miRNAs, and also among members of the same miRNA family (Figure S3). To simplify the expression profiles of DEMs, their dynamic changes in C18 and C6 were categorized into six expression patterns (K1–K6) (Figure 2c, Table S2): K1 elevated expression at 1–14 DAC but reduced at 21 DAC; K2 induced expression at 7 DAC, then downregulated at 14 and 21 DAC; K3 induced expression till 7 DAC, then downregulated at 14 and 21 DAC; K4 the rising trend in C18 stopped at 1 DAC, followed by a downregulation until 14 DAC; K5 downregulation of expression from 1 to 21 DAC; K6 downregulated at 7 DAC, but induced at 14 DAC. Compared with C18, K3 in C6 showed an earlier induction at 1 DAC and then downregulated continuously; K4 in C6 kept rising after cold treatment, which was similar to K1 in C18. A detailed comparison of these co-expressed DEM clusters between C18 and C6 has been illustrated in a Circos diagram, where equivalent overlaps were observed between similar or different clusters (Figure 2c). For example, half of the DEMs from K2 cluster in C18 were also located at the same cluster (K2) in C6, suggesting a shared response mediated by these DEMs against LTs in the two *B. napus* lines. In parallel, DEMs held by K6 cluster of C18 could not be grouped into any clusters of C6, implying divergence in cold adaption between C18 and C6.

DEGs induced by LTs

Global gene expression constitutes another crucial parameter for interpreting cold adaption. Thus, we compared gene expression patterns of LTs on C18 and C6 under the same conditions. On the

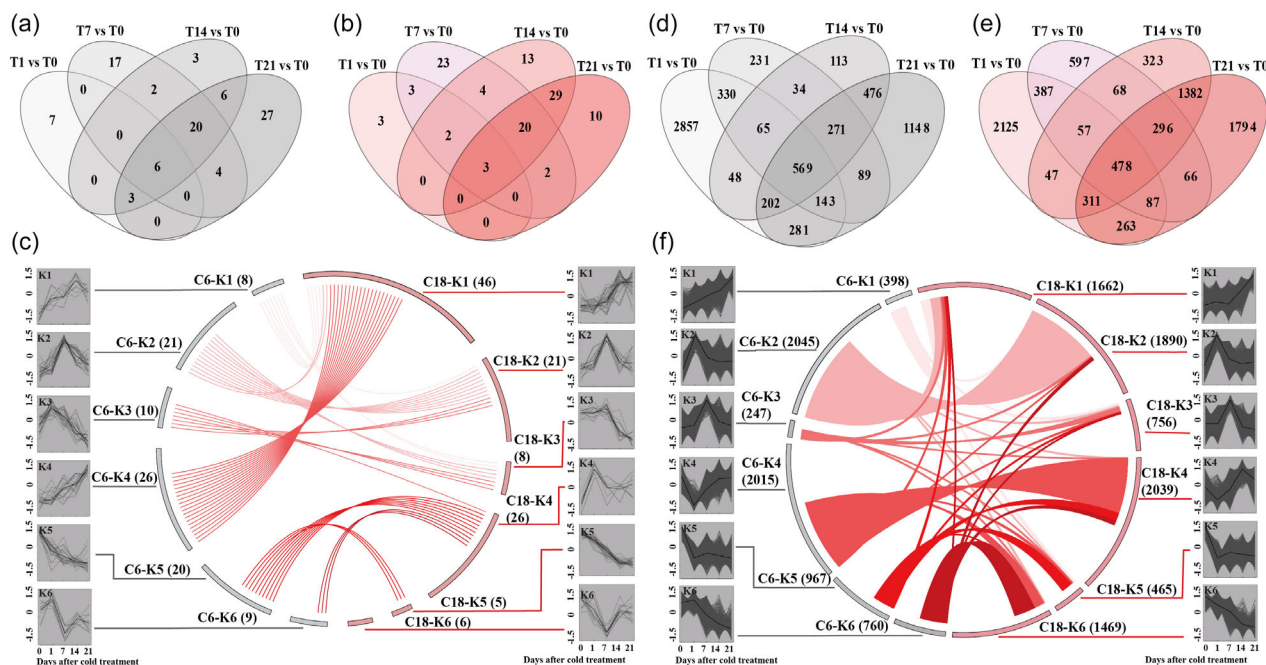


Figure 2 Differentially expressed miRNAs (DEMs) and genes (DEGs) induced by low temperatures (LTs). Venn diagrams of mutual differentially expressed miRNAs (DEMs) (a, b) and differentially expressed genes (DEGs) (d, e) in C6 (grey) and C18 (red). Numbers in each circle indicate total amount of DEMs/DEGs detected at designated time point versus T0, while the numbers in overlapping areas are the amount of shared DEMs/DEGs. (c) and (f) represent six different expression clusters (C6-1 to C6-6, C18-1 to C18-6) of DEMs and DEGs grouped by K-means. Grey lines represent normalized log₂FPKM value of individual DEMs (c) and DEGs (f), while the dark lines indicate means of all DEMs/DEGs in the plot. The number of DEMs/DEGs belonging to each cluster is shown in parentheses. Circos diagrams display the agreement of each cluster by LTs between C6 (the left side) and C18 (the right side). Ribbons within the Circos diagram connected mutual DEMs/DEGs.

basis of bioinformatic analysis, 11 142 DEGs were identified and categorized in Venn diagrams (Figure 2d,e): these included 8281 and 6432 DEGs in C18 and C6, respectively. The MA-plots and volcano plots showed that the number of upregulated genes were close to that of down-regulated genes in most comparisons (Figure S4). Based on the kinetic expression patterns, these DEGs were clustered into six expression patterns (Figure 2f, Table S3). K1 exhibited a continuously rising expression pattern, while K2 and K3 showed a single peak at 1 DAC and 7 DAC, respectively. The expression of DEGs belonging to K4 increased after an initial decrease, while K5 significantly decreased at 1 DAC; besides, K6 exhibited a continuously declining expression pattern. A limited overlap was observed between similar clusters, which accounted for approximately 60% of the DEGs, for example, K2 cluster, suggesting that these kinds of responses were conserved between the two *B. napus* varieties. It is worthwhile to mention that a considerable fraction of DEGs showed different expression patterns in C18 and C6. We hypothesize that these DEGs might be the reason for C18 and C6 to respond distinctively to LT stress. We then examined the changes in the relative abundance of typical cold-responsive genes (Figure S5). The cold related marker genes (*CBF5*, *CBF7*, *COR25*, *COR115*) and six randomly selected genes showed consistency between the qPCR assays and the RNA-Seq data in terms of the direction of regulation and statistical significance.

To explore the relationship between DEGs and cold adaption in *B. napus*, we applied GO and KEGG pathway analysis, respectively. Pathways with a corrected *P*-value of <0.05 were summarized in a heat map, which highlighted the conserved or specific biological processes during LT stress treatment. Overall, carbohydrate and polysaccharide metabolic processes were enriched in both varieties, whereas specific enriched pathways were detected at different time points between C18 and C6 (Figure S6a). Most GO terms were significantly overrepresented in C18 than in C6, except in the case of the T_1/T_0 comparison (Figure S6b), indicating that the reactions probably differ between the cold sensitive and tolerant varieties, and wider responses were triggered in the tolerant variety.

Potential DE miRNA-target modules

Having obtained both miRNA and mRNA profiles from the same samples, we investigated target genes for DEMs. A total of 8685 genes (5409 in C18, 6407 in C6) were predicted to be the targets of all DEMs with high confidence (<http://plantgrn.noble.org/psRNATarget>) (Table S4). A summarized heat map revealed the diverse expression patterns of these target genes (Figure S7). 8.4% of these target genes were differentially expressed in C18, compared to 5.8% in C6, designated as DE-targets (Table S5). This includes 457 DEGs targeted by 112 DEMs of C18, followed by 370 DEGs targeted by 94 DEMs of C6.

To better correlate DEMs with their target genes, we summarized the DE-target classifications corresponding to each DEM. A high percentage of the DE-targets was grouped to different DEG clusters with the corresponding DEMs (Table S6). For accurate construction of the miRNA-target modules, a strong anti-correlation (Pearson correlation ≤ -0.7) within DE-targets and DEMs was set as the threshold using SPSS software (Woo et al., 2016), resulting in 58 and 53 potential DEM-target modules in C18 and C6, respectively. Out of these, six potential modules were shared between C18 and C6. A detailed list of DEMs and corresponding DE target genes is outlined in Supplementary Table (Table S6). As expected, a set of earlier

reported pathways were detected in our study, including *miR164*–NAC (Lu et al., 2017) and *miR172*–AP2 (Ahmed et al., 2021). Such modules triggered by conserved miRNAs were highlighted in a heat map (Figure 3a), displaying inverted time course of expression between DEMs and corresponding DE-targets.

To confirm the results from the integrated analysis, we examined changes in the relative abundance of representative modules via qRT-PCR (Figure 3b–g); the expression patterns of DE-miRNA or DE-targets fully matched the anti-correlation data. It is worth noting that modules mediated by differentially expressed *Bna-miR397* (including *Bna-miR397a* and *Bna-miR397b*) were depicted in the cold-tolerant variety C18 exclusively. The mature sequences of *Bna-miR397s* (including *miR397a* and *miR397b*) from rapeseed were the same as *miR397a* from *Arabidopsis*, while there were significant differences compared to those of gramineae crops such as rice and wheat (Figure S8). To better understand the function of the predicted DEM-DE target module, we chose *Bna-miR397a* mediated modules for further studies.

The *Bna-miR397a*–*BnaLAC2* module contributes to cold adaptability

Previously, *miR397* has been suggested to be involved in cold acclimation, with varied functional roles specific to the species (Chen et al., 2015; Dong and Pei, 2014; Huo et al., 2022). Here, we found that there is 70% reduction in the *Bna-miR397a* expression level from the susceptible variety C6 compared with the resistant variety C18 under normal growth conditions (Figure 3e). During cold treating period, induction of *Bna-miR397a* in C18 was rapid and more pronounced, more than 6-fold at 21 DAC, whereas the level of *Bna-miR397a* in C6 gradually increased by 1.46-fold during the same period (Figure 3e). Of particular note, *Bna-miR397a* mediated modules, repression of *BnaA05g06610D* (*BnaLAC4-1*), *BnaC04g07220D* (*BnaLAC4-2*), *BnaA02g06580D* (*BnaLAC17*) and *BnaC04g54790D* (*BnaLAC2*), were specifically detected in C18 (Table S6). Thus, the rapid and strong induction of *Bna-miR397a* mediated modules may be associated with C18-specific cold adaptability under long-term exposure.

Bna-miR397a positively modulates cold adaptability of *B. napus*

To further explore the significance of *Bna-miR397a* against cold in *B. napus*, we overexpressed the precursor sequence of *Bna-miR397a*; meanwhile, we inactivated *Bna-miR397a* via STTM (short tandem target mimic) in Westar, a *B. napus* variety moderately sensitive to cold. As expected, the expression of *Bna-miR397a*, compared with wild type (WT) C6, significantly increased in three independent overexpression lines (designated as *Bna-miR397aOE1*–*3*) (Figure 4a), while the expression level of *Bna-miR397a* was repressed to different extents in three independent STTM lines compared to Westar (designated as *Bna-STTM397a-1*–*3*) (Figure 4b).

Under normal conditions, *Bna-miR397aOE* and STTM homozygous lines exhibited growth development characteristics similar to those of corresponding WT (Figure 4c). Upon cold treatment, *Bna-miR397aOE* plants grew better and had larger leaves, with enhanced cold tolerance over WT plants. Overexpression of *Bna-miR397a* significantly inhibited cold-induced EL of leaves, accompanied by higher biomass accumulation and proline contents compared to the corresponding WT (Figure 4d–f). By contrast, repression of *Bna-miR397a* in STTM lines aggravated the

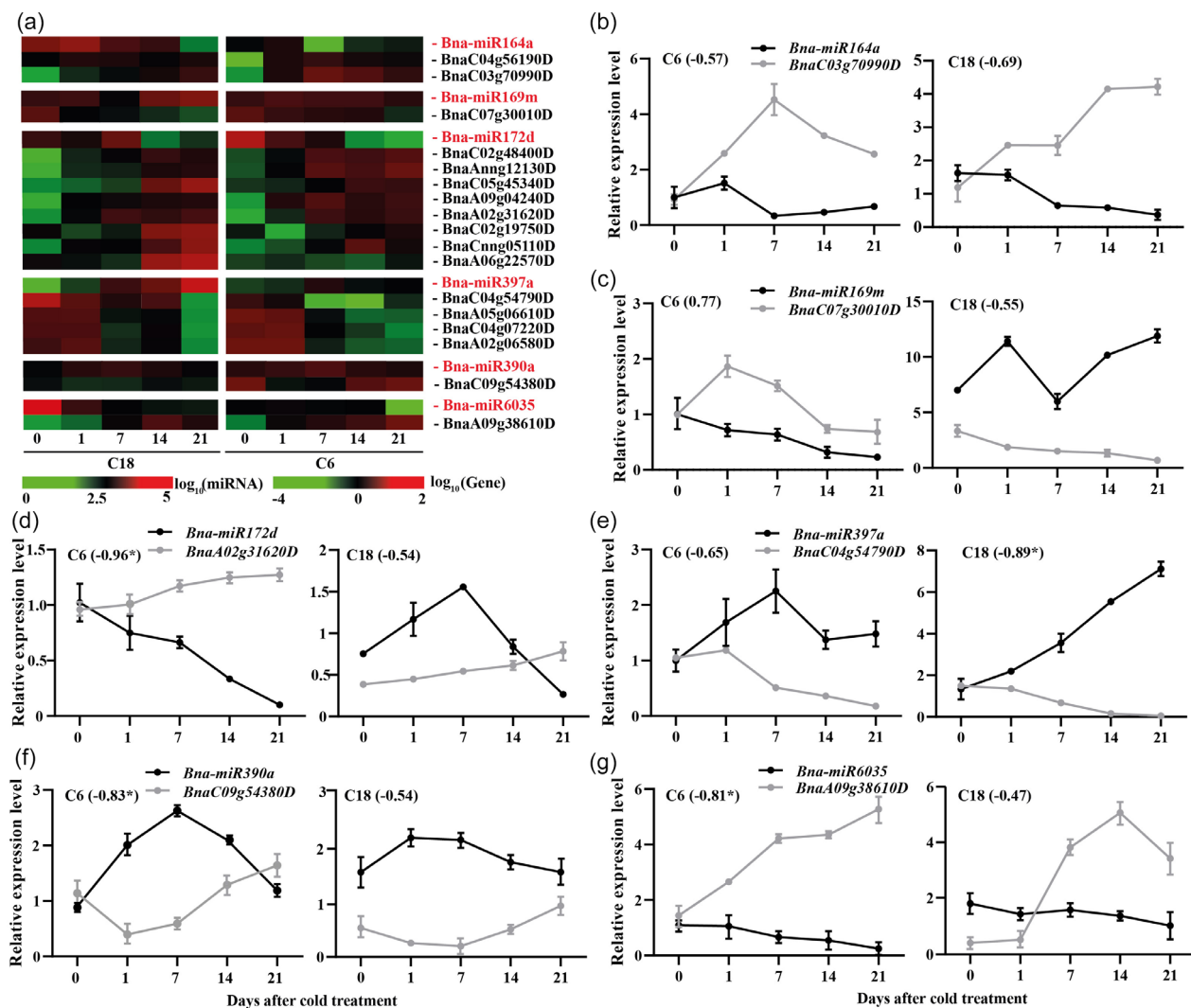


Figure 3 Expression profiles of DE-target based on K-means analyses and qRT-PCR. (a) Heat map of differentially expressed miRNAs (DEMs) and targets signature in *Brassica napus* lines C18 and C6 during cold stress. Target signatures for each DEM are created based on the expression of predicted target genes. Expression of each signature is calculated based on the mean-scaled $\log_{10}(\text{FPKM})$ from RNA-seq data. The colour gradient, ranging from green, through black, to red represents low, middle, high values of the expression. (b–g) qRT-PCR validations of DEMs and corresponding targets from selected modules. The *U6* or *BnaACTIN* genes are used as internal controls for miRNA or target genes expression, respectively. 0, 1, 7, 14, 21 represent 0 day, 1 day, 7 days, 14 days, 21 days after cold treatment. Each data represents the mean \pm standard error (SE) of three replicates.

extent of cold injury, led to a rise in percentage of EL by 5%–8% at 21 DAC. Furthermore, we detected lower levels of proline and biomass accumulation in these STTM lines. These results suggest that *Bna-miR397a* positively modulates the cold adaptability of *B. napus* during long-term LTs stress.

Disruption of *BnaLAC2* enhances cold adaptability of *B. napus*

Bioinformatics analysis revealed that *BnaA05g06610D* (*BnaLAC4-1*), *BnaC04g07220D* (*BnaLAC4-2*), *BnaA02g06580D* (*BnaLAC17*) and *BnaC04g54790D* (*BnaLAC2*) were potential targets of *Bna-miR397a* (Table S6). In addition, the four genes exhibited an inverse expression profile in the resistant variety C18 during long-term cold stress (Table S6). Consistent with that, the *Bna-miR397a*OE plants had lower expression levels of the four genes, while the STTM plants showed higher expression levels of these genes than their corresponding WT, especially in *BnaLAC2*. *BnaLAC2* appeared to be most significantly affected by

Bna-miR397a, with its expression level equivalent to 6.7% of that in WT plants, while the expression levels of the other three genes were equivalent to 25%–40% of WT plants (Figure S9a). After inhibiting *Bna-miR397a*, the expression level of *BnaLAC2* was 23.7 times higher than that of WT plants, while the expression levels of the other three genes only increased by 2.6, 5.0 and 8.7 times when compared to WT plants, respectively.

Similar results were obtained using transient co-expression assays. As expected, *Bna-miR397a* accumulation was induced under the control of the constitutive 35S promoter in WT *B. napus* protoplast, while accumulations of the four genes driven by 35S promoter were greatly downregulated when they were co-expressed with *Bna-miR397a* individually (Figure S9b). Such results indicated that *Bna-miR397a* could trigger the repression of the above four genes in *B. napus*. However, we could only detect a cleavage site in the fifth exon of *BnaLAC2* using RNA ligase-mediated rapid amplification of cDNA ends (RLM-RACE) assays, right after the

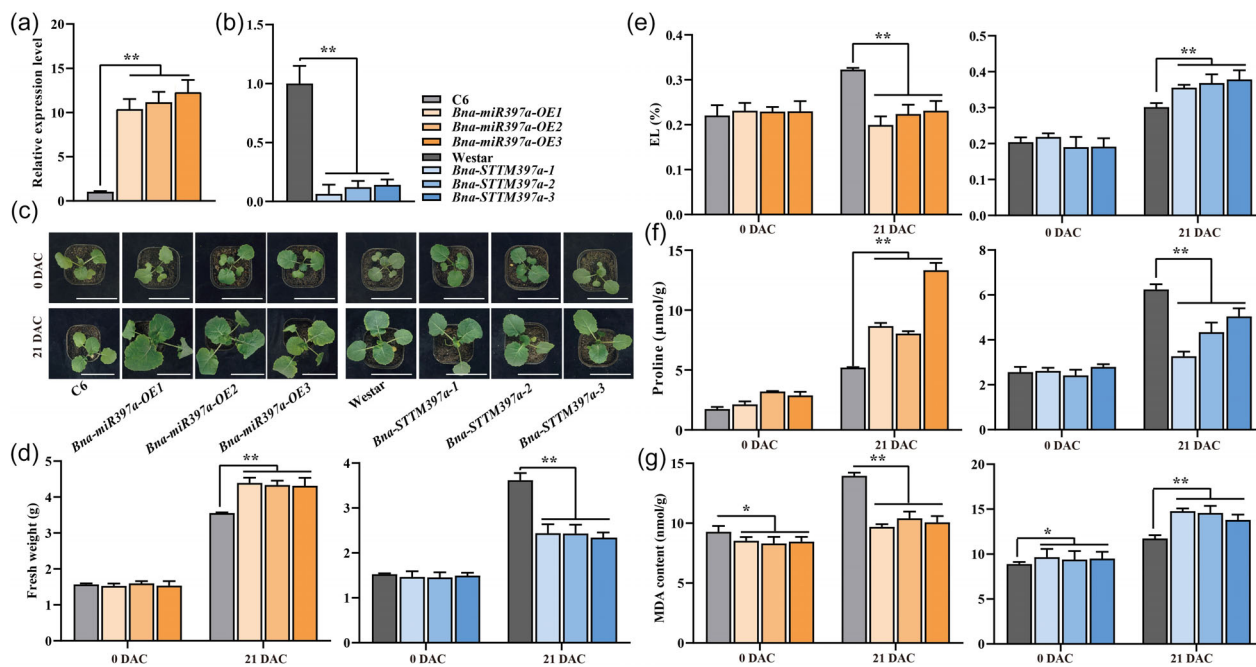


Figure 4 *Bna-miR397a* confers cold tolerance in *Brassica napus*. (a, b) Relative expression levels of *Bna-miR397a* in overexpression, *Bna-STTM397a* lines and the corresponding WT plants. The *U6* or *BnaACTIN* gene are used as internal control for miRNA or target genes expression, respectively. (c) Performance of the transgenic *B. napus* lines (*Bna-miR397aOE*, *Bna-STTM397a*) and WT plants before (0 DAC) and after 21 days (21 DAC) of cold treatment. Determination of the physiological parameters, (d) fresh weight (g), (e) electrolyte leakage (EL, %), (f) proline content ($\mu\text{mol/g}$) and (g) MDA content (nmol/g) of the *Bna-miR397aOE*, *Bna-STTM397a* lines, WT plants before and after cold treatment. Each data represents the mean \pm standard error (SE) of three replicates. Asterisks indicate significant differences compared to the respective wild-type control under the same treatment conditions (* $P < 0.05$, ** $P < 0.01$, Student's *t*-test).

687th nucleotide from ATG (Figure 5a). This site showed 70% complementary to *Bna-miR397a*. A dual-luciferase assay further demonstrates its direct inhibition on *BnaLAC2* transcription. When co-expressed with *BnaLAC2*, *Bna-miR397a* significantly reduces the LUC/REN ratio by 72% (Figure 5b). To determine whether the regulation of *BnaLAC2* is responsible for the cold response, the transcript abundance of *BnaLAC2* was investigated in *Bna-miR397aOE*, *Bna-STTM397a* and corresponding WT plants exposed to cold stress (Figure S9c). We found that the expression of *BnaLAC2* in the *Bna-miR397aOE* lines was much lower than that in WT plants under cold conditions. Moreover, the *Bna-miR397a*-mediated repression under cold conditions was disrupted in *Bna-STTM397a* lines when compared to WT plants.

We then investigated the role of *BnaLAC2* in *B. napus* adaptation to LTs. Two CRISPR/Cas lines of *BnaLAC2* (*Bnalac2*) were generated (Figure 5c). These materials were subjected to the same LT assay. Similar to *Bna-miR397aOE* plants, the *Bnalac2* mutants grew better and had larger leaves after cold stress (Figure 5d). Compared to WT plants, accumulations of biomass and proline contents were higher in *Bnalac2* mutants, similarly, the percentage of EL in the two independent knock-out lines maintained at a relatively stable state during LTs stress (Figure 5e–g), suggesting that *BnaLAC2* is a negative regulator of LT tolerance in rapeseed. Therefore, it is concluded that *Bna-miR397a* can mediate resistance against LT by disruption of *BnaLAC2*.

***Bna-miR397a*–*BnaLAC2* mediated cold adaptability is associated with lignin biosynthesis modulation**

As *miR397* has been shown to modulate the lignin biosynthesis regulatory pathway in both herbaceous and woody plants species

(Khandal et al., 2020; Wang et al., 2014a), we hypothesized that the *Bna-miR397a*–*BnaLAC2* module could influence lignin accumulation in *B. napus* under cold conditions. To test this hypothesis, stem cross-sections from the respective plant lines were stained with phloroglucinol-HCl. Irrespective of the growth conditions, the pink or fuchsia staining, indicative of lignifying cells, was less intense in *Bna-miR397aOE* and *Bnalac2* lines compared to corresponding WT plants, while being more pronounced in *Bna-STTM397a* lines (Figure 6a,b). Subsequent quantification of lignin content corroborated the staining results, indicating a significant influence of the *Bna-miR397a*–*BnaLAC2* module on lignin accumulation in *B. napus*. Overexpression of *Bna-miR397a* or knockout of *BnaLAC2* resulted in decreased total lignin content compared to the corresponding WT plants, whereas silencing of *Bna-miR397a* led to increased lignin content (Figure 6c). This effect was consistently observed under cold stress conditions. Prolonged cold treatment alone significantly affected lignin content in rapeseed cell walls. In C6 plants, cold stress induced a gradual reduction in lignin content, followed by a gradual recovery during the subsequent recovery period (Figure 6c, Figure S10a). Prior to cold treatment, *Bna-miR397aOE* and *Bnalac2* lines exhibited 12.7% and 16.2% lower lignin levels than the corresponding WT plants, respectively, whereas *Bna-STTM397a* lines displayed a 16.2% increase in lignin content. Although cold stress reduced lignin content across all lines, *Bna-miR397aOE* and *Bnalac2* lines consistently exhibited lower levels than the corresponding WT, whereas *Bna-STTM397a* lines consistently exhibited higher levels. As the cold-tolerant variety, C18 also showed 13.5% reduction in lignin content than C6 (Figure S10b). Following a 7-day recovery period, lignin content in

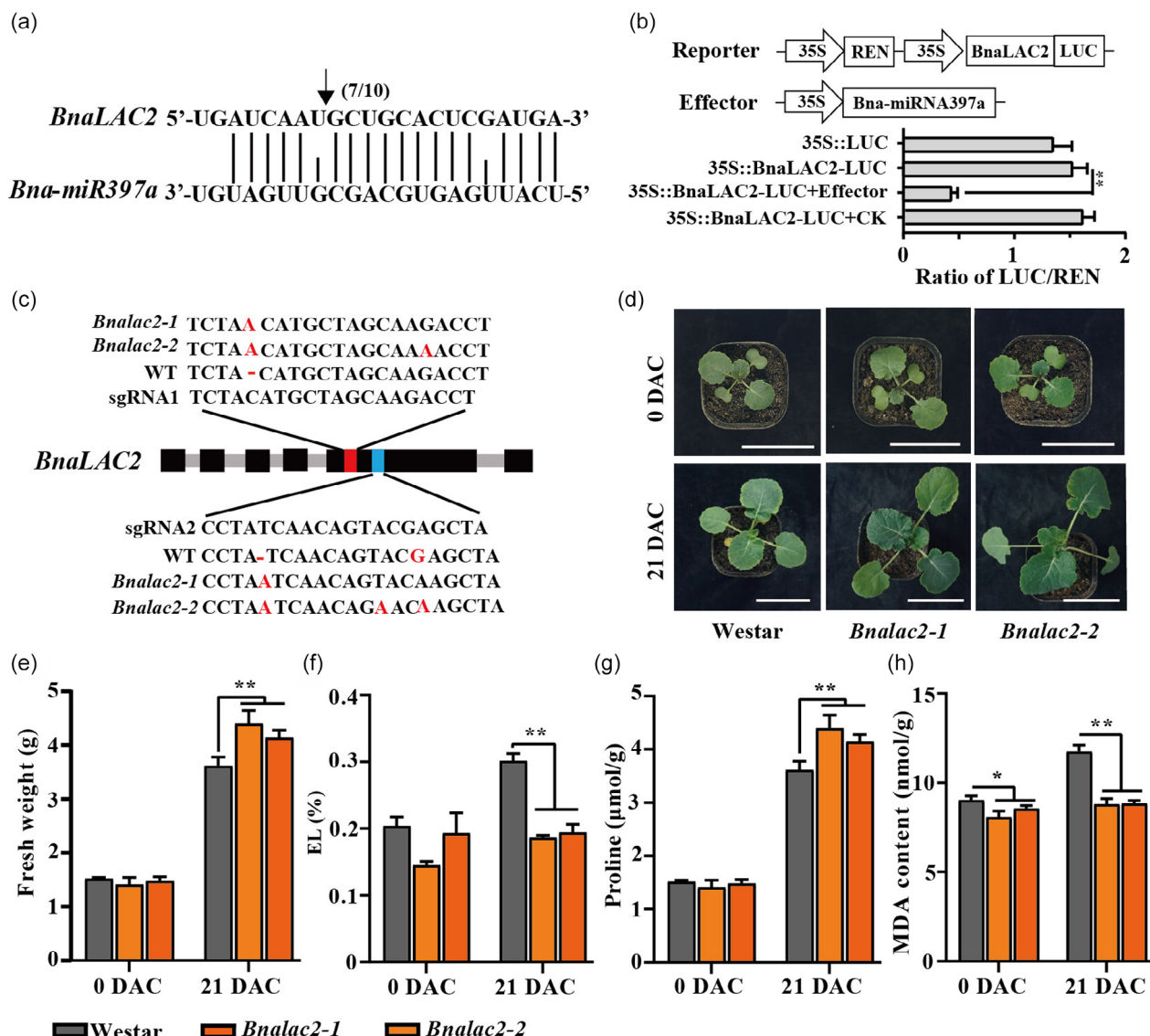


Figure 5 *BnaLAC2*, a target of *Bna-miR397a*, confers cold sensitivity in *B. napus*. (a) Cleavage of *BnaLAC2* mRNA by *Bna-miR397a*. The cleavage site within the *BnaLAC2* mRNA was determined using 5' RACE analysis. (b) Dual-luciferase assay in *Nicotiana benthamiana* leaves. The ratio of firefly luciferase (LUC) to Renilla luciferase (REN) activity was measured in leaf tissue co-infiltrated with constructs expressing *Bna-miR397a* and *BnaLAC2*. pGreenII 62-SK with or without the *Bna-miR397a* insert served as the effector and negative control (CK), respectively. A schematic representation of the effector and reporter constructs is shown above the graph. (c) CRISPR/Cas9-mediated mutagenesis of *BnaLAC2*. The target sites for two single guide RNAs (sgRNA1, sgRNA2) designed to generate mutations in the *BnaLAC2* gene are shown. Sequence alignment of the target region confirmed homozygous insertion of an adenine base in two independent mutant lines (*Bnalac2-1*, *Bnalac2-2*). (d) Performance of *Bnalac2-1*, *Bnalac2-2* and WT plants under cold stress. Plants were subjected to a 21-day cold treatment, and the following physiological parameters were measured before and after treatment: (e) fresh weight (g), (f) electrolyte leakage (EL, %), (g) proline content (μmol/g) and (h) MDA content (nmol/g). Each data represents the mean ± standard error (SE) of three replicates. Asterisks indicate significant differences compared to the respective wild-type control under the same treatment conditions (* $P < 0.05$, ** $P < 0.01$, Student's *t*-test).

all lines returned to levels comparable to those observed before cold treatment; however, the differences in lignin content between the transgenic lines and the WT remained consistent throughout the experiment.

It is well established that LACs genes polymerize the monolignols into lignin, which is composed of syringyl (S), guaiacyl (G) and p-hydroxyphenyl (H) units (Quan *et al.*, 2019). We then examined whether lignin composition was altered in *Bna-miR397a* related plants (Figure 6d, Table S7). Under normal growth conditions, the levels of G and S lignin units were

comparable, while H units were present in lower amounts. Compared to the corresponding WT plants, both *Bna-miR397a*OE lines and the *Bnalac2* mutant exhibited reductions in all three lignin monomers, with the *Bnalac2* mutant displaying more pronounced decreases. In contrast, the *Bna-STTM397a* lines exhibited increased levels of all three monomers. Specifically, compared to the wild type, G, S and H unit content decreased by an average of 8.5%, 14.5% and 27.24% in *Bna-miR397a*OE lines; 15.3%, 17.9% and 43.2% in the *Bnalac2* mutant; and increased by 12.7%, 20.0% and 42.1% in the *Bna-STTM397a*

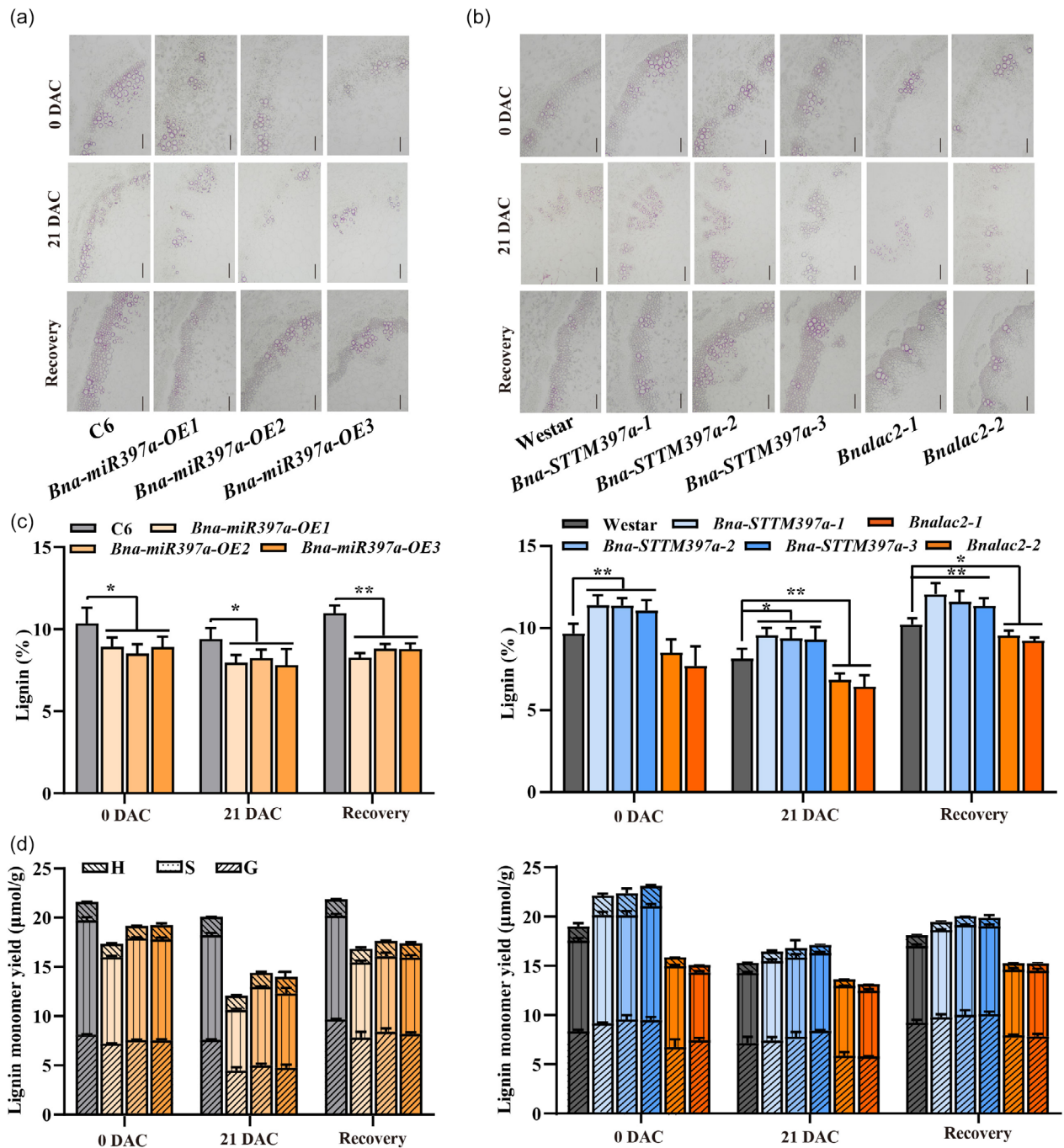


Figure 6 The *Bna-miR397a-BnaLAC2* module regulates lignin biosynthesis in *Brassica napus* under cold stress. (a, b) Representative micrographs of stem cross-sections from *B. napus* lines stained with phloroglucinol-HCl to visualize lignin deposition. Images were taken before cold treatment (0 DAC), after 21 days of cold treatment (21 DAC) and after 7 days of recovery (Recovery). (a) Wild-type (C6) and *Bna-miR397a* overexpression (OE) lines. (b) Wild-type (Westar), *Bna-STTM397a* (target mimicry of *miR397a*) lines and *Bnalac2* mutant lines. Scale bar = 2 μm . (c, d) Quantification of lignin content (c) and lignin monomer composition (d), specifically the relative abundance of p-hydroxyphenyl (H), syringyl (S) and guaiacyl (G) subunits, in the indicated *B. napus* lines under the same cold treatment and recovery conditions as in (a, b). Each data represents the mean \pm standard error (SE) of three biological replicates. Asterisks indicate significant differences compared to the respective wild-type control under the same treatment conditions (* $P < 0.05$, ** $P < 0.01$, Student's *t*-test).

lines, respectively. These results suggest that the *Bna-miR397a-BnaLAC2* module is involved in regulating lignin biosynthesis under normal growth conditions, differentially affecting the various monomers. Specifically, the H unit is most affected, followed by the S unit and lastly, the G unit.

Following 21 days of cold treatment, a decrease in the levels of all three lignin monomers was observed across all lines (Table S7). In both *BnamRNA397aOE* and *Bnalac2* mutants, the reduction rate of G units surpassed that of S units. Conversely, in the *Bna-STTM397a* lines, the H unit exhibited the most substantial

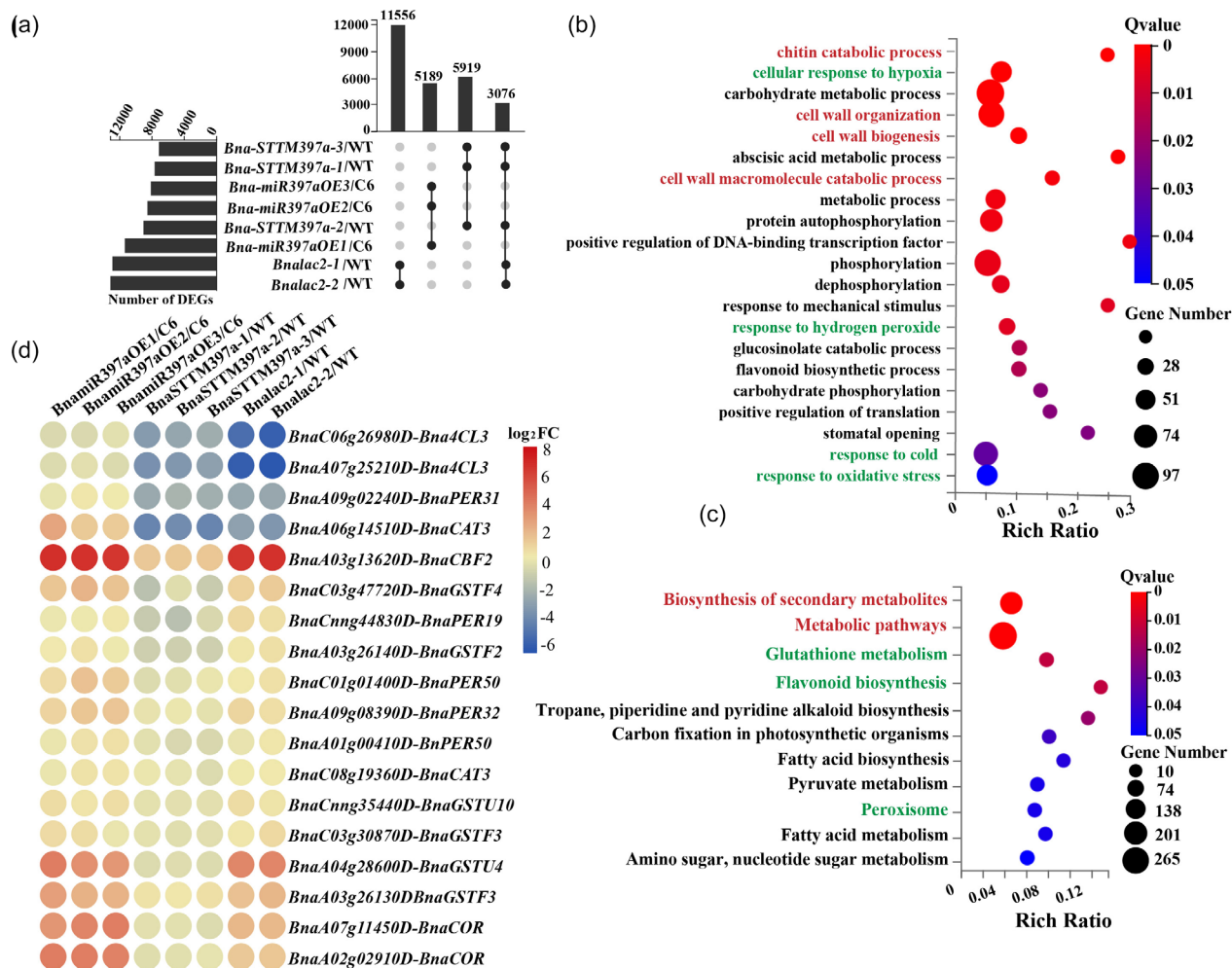


Figure 7 Global transcriptome changes affected by the *Bna-miR397a-Bnalac2* module under cold stress. (a) The comparison of differentially expressed genes (DEGs) between indicated comparisons. DEGs were identified using \log_2 fold change (\log_2FC) threshold ≥ 1 and a significance level of $P < 0.05$. GO-biological process (BP) enrichment (b), and KEGG pathway enrichment (c) of 3067 overlapped DEGs. (d) Heatmap showing the related genes regulated by *Bna-miR397a-Bnalac2* using \log_2FC .

decrease (an average reduction of 55.4%), followed by S units and lastly, G units. This observation is consistent with the varying sensitivities of the three monomers to the *Bna-miR397a-BnaLAC2* module observed under normal growth conditions. During the recovery period, G unit content rapidly increased in *Bna-miR397aOE* and *Bnalac2* mutant lines, exhibiting average increases of 71.6% and 35.3% compared to relative to the G unit levels at the end of the 21-day cold treatment, respectively. Conversely, the *Bna-STTM397a* lines and the wild type displayed similar G unit increases (26.8% and 28.7%, respectively).

Monolignol synthesis and lignin deposition occur in multiple steps that involve several enzymes. Thus, we further investigated the expression of some genes involved in the monolignol biosynthesis pathway (Figure S11). The *Bna-miR397a* transgenic plants and *Bnalac2* mutants displayed no significant modification of the expression level of these genes before cold stress, except for repression of *CCR2* in *Bna-miR397aOE* plants. After cold stress, however, *Bna-miR397aOE* plants and *Bnalac2* mutants displayed increases in the expression of *C4H*, *CAD*, *CCR2*, *HCT* involved in lignin biosynthesis, suggesting the *Bna-miR397a-BnaLAC2* module has a positive feedback on the regulation of monolignol synthesis.

Bna-miR397a-BnaLAC2 mediated cold adaptability is associated with ROS homeostasis

To investigate the molecular mechanisms underlying the synergistic regulation of cold tolerance by the *Bna-miRNA397a-BaLAC2*, we performed RNA-Seq analysis on the different transgenic lines following cold treatment. We first analysed lines sharing the same genetic background. As depicted in Figure 7a, the Venn diagram illustrates that 3076 DEGs were shared between the *Bna-STTM397a* line and the two *Bnalac2* mutant lines. GO enrichment analysis revealed that, in addition to the enrichment of the 'response to cold' biological process, biological processes related to the cell wall were prominently represented during cold treatment (Figure 7b, Table S8), including 'cell wall organization or biogenesis', 'chitin catabolic process', 'cell wall biogenesis' and 'cell wall macromolecule metabolic process'. These results suggest that cell wall remodelling is an important mechanism by which the *Bna-miRNA397a-BnaLAC2* module mediates responses to cold stress. Furthermore, genes belonging to the enriched 'response to cold' pathway suggests that osmotic adjustment also contributes to the cold stress response in *B. napus*.

Additionally, KEGG enrichment analysis revealed significant enrichment of the 'glutathione metabolism' and 'flavonoid biosynthesis' pathways, with the 'response to oxidative stress', 'cellular response to hypoxia' etc. also being enriched in the GO analysis (Figure 7c, Table S8). Among DEGs belonging to above clusters, 18 members were also significantly altered in *Bna-miR397aOE* lines at 21 DAC (Figure 7d).

Glutathione and flavonoids, as key antioxidants, scavenge reactive oxygen species (ROS), suggesting a potential role for ROS in cold tolerance. However, the interplay between ROS and cold stress response is complex. Although cold stress typically triggers ROS accumulation, inducing cell wall remodelling as a defence mechanism (Kutsuno et al., 2023; Tenhaken, 2014), alterations in cell wall structure (e.g. lignin modifications) can disrupt ROS homeostasis (Wang et al., 2021). Consequently, we investigated how the *Bna-miR397a-BnaLAC2* module influences this intricate interplay between cold tolerance and ROS homeostasis.

Compared to the cold-sensitive wild type (C6), the cold-resistant *Bna-miR397a-OE* lines consistently exhibited lower H₂O₂ and malondialdehyde (MDA) levels (Figure 4g, Figure S12), both before and after prolonged cold treatment. This lower increase indicated an enhanced ability to mitigate oxidative damage under cold stress. They also displayed significantly higher GST activity, suggesting a superior detoxification capacity. Higher POD and CAT activities at 21 DAC further demonstrated enhanced ROS scavenging. In contrast, the *Bna-STTM397a* lines exhibited higher MDA and H₂O₂ levels compared to Westar, likely due to generally lower enzyme activities. Histochemical staining (Figure S12) corroborated these findings, with less H₂O₂ accumulation in the resistant *Bna-miR397a-OE* and *Bnalac2* lines. qRT-PCR analyses of ROS-related genes (*GSTs*, *PERs*, *CATs*) were consistent with RNA-Seq data (Figure S13), suggesting that *Bna-miR397a* overexpression enhances ROS scavenging efficiency. Interestingly, despite lower POD activity, the cold-tolerant *Bnalac2* mutant displayed higher GST activity, potentially mitigating downstream ROS damage by detoxifying secondary oxidative stress products (Kumar and Trivedi, 2018). Furthermore, the expression of specific COR genes (*CBF2*, *COR6.6*, *COR25*, *COR115*) was significantly upregulated in the *Bnalac2* mutant line (Figure S14). Thus, the data indicates that *Bna-miR397a-BnaLAC2* mediated cold adaptability is associated with enhanced ROS scavenging system and CBF/DREBs pathway.

***Bna-miR397a-BnaLAC2* positively regulate freezing tolerance**

To gain further insights into the biological function of *Bna-miR397a-BnaLAC2* in freezing tolerance, the aforementioned plants were further exposed to freezing stress (−4 °C). After 4 h treatment, *Bna-miR397aOE* and *Bnalac2* mutants significantly enhanced freezing tolerance, with the survival rate increasing by 70% and 27%, respectively, compared to corresponding WT plants (Figure 8a,b). While STTM lines were more sensitive to freezing stress and showed more injured seedlings, the survival rate was 40% lower than the WT plants (Figure 8d,e). EL assays indicated that plasma membrane damage caused by freezing stress was greatly reduced in *Bna-miR397aOE* and *Bnalac2* mutants but increased in STTM lines (Figure 8c,f).

Since the mature sequence of *Bna-miR397a* was identical to *miR397a* from *Arabidopsis*, we then examined whether the *miR397-LAC2* module plays a conserved role in *Arabidopsis*. As overexpressing *At-miR397a* exhibits enhanced cold hardiness of *Arabidopsis* (Dong and Pei, 2014), transgenic plants designated as

miR397aOE and *At-STTM397a* (*STTM397a*) were generated by overexpressing the precursor sequence of *Bna-miR397a* and STTM technology. The expression levels of *miR397a* were dramatically increased in *miR397aOE* and reduced in *STTM397a* plants (Figure S15a). Meanwhile, one homozygous T-DNA insertion mutant (SALK_025690C) for *Atlac2* (*lac2*) was obtained. The expression level of *AtLAC2* was significantly reduced in the mutant compared to the WT plants (Figure S15b). Under freezing conditions (−4 °C), the two lines of *STTM397a* and WT plants severely wilted and displayed injury, while two lines of *miR397aOE* and *lac2* mutants appeared to be much healthier (Figure S15c). The phenotype difference was further quantified based on the stress-induced EL assay and freezing survival rate (Figure S15d,e). The above results indicate the *miR397a-LAC2* module conservatively functions in the adaption of *Cruciferae* to LT stress (Figure 9).

Discussion

The advantages of leveraging combined omics to dissect complex traits

A major goal of current agricultural research in *B. napus* is the enhancement of cold tolerance. Specifically, identifying cold-tolerant germplasm and elucidating the underlying cold response mechanisms are critical. Recent years have witnessed significant advances in our understanding of the molecular mechanisms underlying cold adaptation, largely attributed to the advent of high-throughput experimental approaches. However, the precise cold-associated functions of several non-coding RNAs, particularly miRNAs and long non-coding RNAs (lncRNAs), remain to be fully elucidated. Considerable research efforts have focused on investigating cold-responsive genes and sRNAs in *B. napus* (Ke et al., 2020; Luo et al., 2019). For instance, a transcriptomic study on the *B. napus* line '2016TS (G)10' under −2 °C freezing stress conditions identified 3905 DEGs, with 2312 upregulated and 1593 down-regulated (Pu et al., 2019). Similarly, sRNA-seq analysis of a spring-type line of *B. napus* subjected to 48 h of cold stress (4 °C) revealed 129 differentially expressed miRNAs (DEMs): 105 non-conserved and 24 conserved (Megha et al., 2018). Considering the spatial and temporal variability of miRNAs in the cold response, extensive further research is necessary before the full potential of natural or artificial miRNAs can be harnessed to enhance crop traits. Furthermore, the aforementioned studies, while insightful, primarily focused on independent analyses of either the transcriptome or sRNAome. Consequently, the precise correlations underpinning miRNA-mRNA interactions remain to be elucidated. The omics approach presents a compelling tool for obtaining a comprehensive understanding of diverse biological processes and is widely recognized as a powerful means of systematically identifying the key genes, pathways and networks underpinning complex traits (Yang, 2022). Integrated omics analyses, such as transcriptomic and sRNA-omic analyses, have recently demonstrated their utility in characterizing miRNA-mediated modules in plants. An integrated miRNA-mRNA expression profiling analysis identified 302 DEMs and 351 potential target genes in response to infection by rice black-streaked dwarf virus in maize, and six miRNA-mRNA modules were found to play key roles in defence (Li et al., 2018). In *B. napus*, mRNA and small RNA sequencing was conducted to reveal the mechanisms influencing harvest index during the seed-filling stage. The *Bna-miR396-Bna.A06SRp34a/Bna.A01EMB 3119* pair, combined with the co-expression network, was found

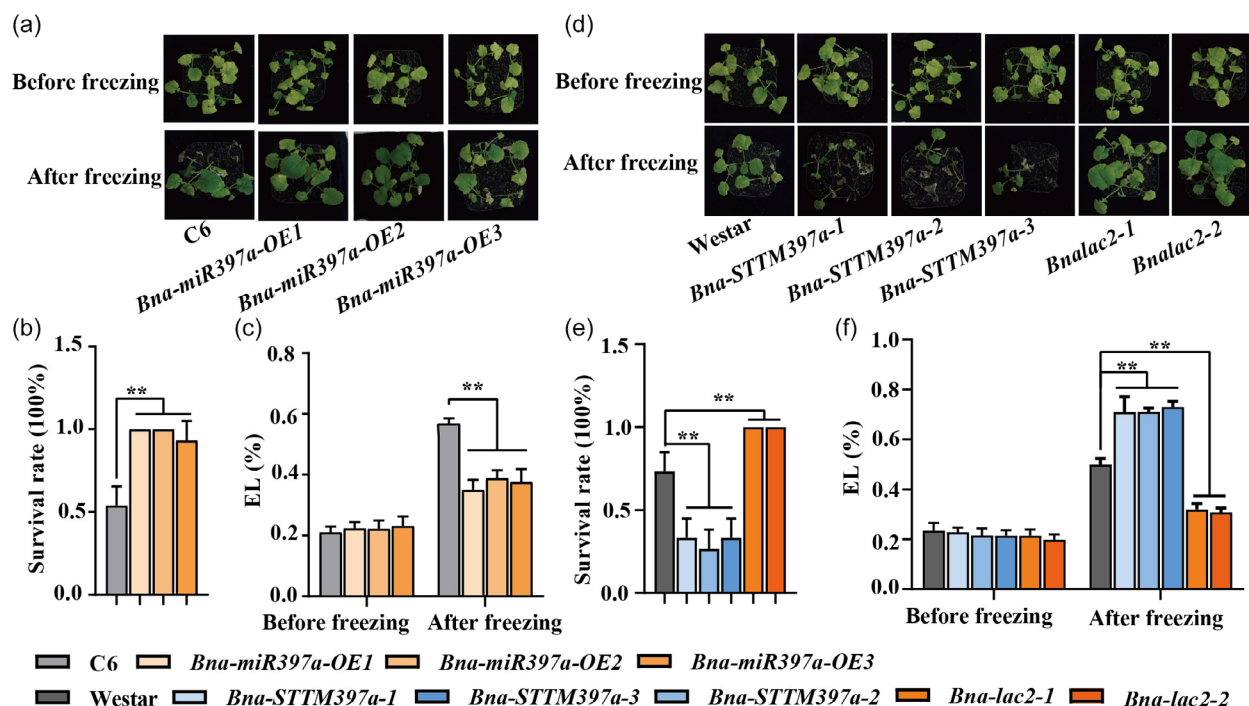


Figure 8 *Bna-miR397a*–*BnaLAC2* confers freezing tolerance in *Brassica napus*. Performance of the *Bna-miR397a*OE lines (a), *Bna-STTM397a* lines and *Bnalac2* mutants (d) before and after freezing treatment. Determination of survival rate (b) and (e), electrolyte leakage (EL, %) (c) and (f) of the *Bna-miR397a*OE, *Bna-STTM397a* and *Bnalac2* mutants during freezing treatment. Each data represents the mean \pm standard error (SE) of three biological replicates. Asterisks indicate significant differences compared to the respective wild-type control under the same treatment conditions (** $P < 0.01$, Student's *t*-test).

to control seed development and the accumulation of storage compounds (Zhang *et al.*, 2022a).

In this study, a comprehensive co-analysis was conducted on the post-transcriptional regulators (miRNAs) and mRNA transcriptome of the two *B. napus* varieties under long-term cold treatment. Furthermore, the expression patterns of DEMs and DEGs were categorized into six distinct groups (Tables S2 and S3). Significant overlap was observed between the majority of clusters in C18 and C6, implying potentially similar or distinct responses of the two varieties to cold treatment. The identification of 106 miRNA-mediated modules within the two varieties (Table S6) was facilitated by the inverse correlation observed between a set of highly expressed miRNAs, including *Bna-miR164*, *Bna-miR172* and *Bna-miR397*, and their predicted target genes. Most of miRNA-mediated modules were variety-specific, with only six modules shared between C18 and C6. This finding suggests that *B. napus* plants with different genetic backgrounds have evolved distinct systems for optimizing various biological processes during continuous and phased cold response. To our knowledge, this study represents the first attempt to integrate sRNAome and transcriptome analyses of seedlings exposed to long-term cold stress. These established global datasets, particularly the conserved or specific miRNA-target interactions, provide a comprehensive resource for dissecting similar or distinct biological processes in contrasting *B. napus* genotypes following long-term cold acclimation. A subset of these modules has been experimentally validated. For instance, the *NAC1* transcription factor, which is involved in auxin-mediated lateral root formation, is post-transcriptionally regulated by *miR164* (Guo *et al.*, 2005; Li *et al.*, 2012). In our study, *BnaC03g70990D*, annotated as a

homologue of *NAC1*, was identified as a target of *Bna-miR164a* in *B. napus* variety C6 (Figure 3b), was upregulated at 7 DAC but down-regulated at 14 DAC, which was consistent with the limited growth of C6 during cold treatment. In apple (*Malus domestica*), *Mdm-miR172* acts as a positive regulator of cold tolerance (Shen *et al.*, 2023). In the present study, *Bna-miR172d* exhibited a continuously declining expression pattern in C6 during cold treatment, whereas C18 exhibited a rising trend that stopped at 7 DAC, followed by downregulation until 21 DAC (Figure 3d, Table S6). These contrasting expression patterns may be associated with phenotypic differences between C18 and C6. The role of these modules in regulating cold adaptation warrants further investigation to determine whether a direct association exists between predicted modules and cold adaptation, as indicated in Table S6. Overall, integrating the sRNAome and transcriptome data allowed us to generate testable hypotheses regarding the roles of reported miRNA-mediated modules in cold response. Moreover, we propose that the identification of novel miRNA-mediated modules could provide further mechanistic insights into long-term cold stress tolerance.

Complex relationship between lignin remodelling and cold tolerance

Prior research has established the role of the *miR397*–*LAC* module in lignin biosynthesis and various plant processes (Gaddam *et al.*, 2024; Khandal *et al.*, 2020; Yu *et al.*, 2024; Zhang *et al.*, 2013; Zhong *et al.*, 2020), but its specific role in conferring cold tolerance varies across plant species (Dong and Pei, 2014; Gupta *et al.*, 2014). Our study reveals a critical link between cold adaptation and lignin biosynthesis at the seedling stage of

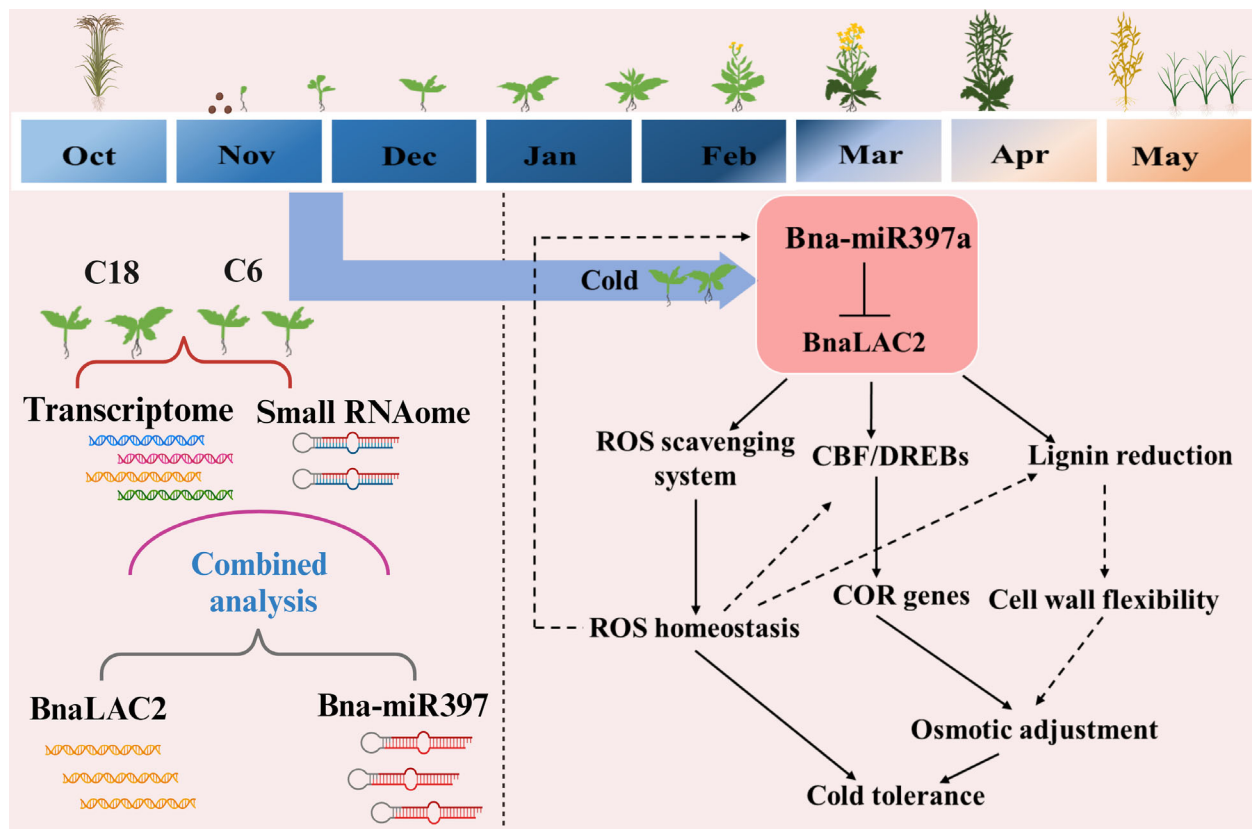


Figure 9 A proposed model of *Bna-miR397a-BnaLAC2* module contributes to cold tolerance under long-term LT stress. The sowing time for *Brassica napus* has recently shifted from October to November due to the delayed harvest of late rice crops. This shift exposes *B. napus* seedlings to increased cold stress during November and December, significantly impacting seed emergence and early plant growth. To identify cold tolerance genes and improve cold tolerance in *B. napus*, a cross-comparison of messenger RNA and small RNA profiles was conducted, leading to the identification of the *Bna-miR397-BnaLAC2* regulatory module uniquely present in the elite breeding line, C18. This module operates through a mechanism whereby *Bna-miR397a* directs the cleavage of *BnaLAC2* mRNA, effectively suppressing the expression of *BnaLAC* genes. Consequently, this suppression results in the inhibition of lignin accumulation, which may contribute to cold tolerance in *B. napus*. These changes ultimately engender cold adaptability in the elite *B. napus* variety C18. Similarly, the miR397-mediated pathway has also been proved to improve freezing tolerance in *Arabidopsis*, indicating a conserved role of miR397-LAC2 in plants. Thus, the integrated multi-omics analysis provides a facile approach to examining the post-transcriptional regulations under long-term cold stress conditions, which highlights the contribution of the *Bna-miR397a-BnaLAC2* module that may be utilized in crop breeding to enhance LT adaption to adverse field conditions, and, more importantly, ensures rapeseed production in the 'rice-rice-rapeseed' triple-cropping system. Solid line indicates direct action, while dotted line indicates multiple steps of action may be required and to be confirmed.

B. napus, mediated by the *Bna-miR397a-BnaLAC2* module. We demonstrate that both overexpression of *Bna-miR397a* and knockout of *BnaLAC2* consistently decrease lignin content while silencing *Bna-miR397a* increases it, indicating a negative regulatory role of this module in *B. napus* lignin biosynthesis. Notably, this regulation is not uniform across all lignin monomers. Under normal growth conditions, H units are most strongly affected, followed by S units and lastly G units. Under cold stress, the impact of the *Bna-miR397a-BnaLAC2* module on lignin monomer composition becomes more specific: overexpressing *Bna-miR397a* or knocking out *BnaLAC2* primarily reduces G unit content, while silencing *Bna-miR397a* primarily affects H units (Figure 6d, Table S7). Furthermore, during the recovery phase following cold stress, these lines exhibit a rapid increase in G unit content, in contrast to the slower increase observed in *Bna-STTM397a* and wild-type plants. This dynamic response suggests that the *Bna-miR397a-BnaLAC2* module appears to contribute to cold tolerance by dynamically regulating lignin composition, particularly G unit abundance and thus modulating cell wall properties.

The G lignin unit, characterized by a single methoxy group ($-\text{OCH}_3$) and a single hydroxyl group ($-\text{OH}$) attached to its aromatic ring, promotes a higher cross-linking density within the lignin polymer. Increased cross-linking contributes to enhanced rigidity and mechanical strength of the cell wall. In contrast, the S unit, sharing the same phenylpropane backbone but containing two methoxy groups ($-\text{OCH}_3$) and one hydroxyl group, forms lignin polymers with less cross-linking than G units, resulting in a more linear and flexible cell wall structure (Barros et al., 2019; Leplé et al., 2007). Following long-term cold treatment, a significant reduction in G unit content was observed in *Bna-miR397aOE* and *Bnalac2* lines, leading to an increased S/G ratio in lignin composition compared to wild-type plants. Based on previous findings linking higher S/G ratios to increased cell wall flexibility (Guo et al., 2001, 2023), the observed shift in lignin monomer composition in *Bna-miR397aOE* and *Bnalac2* lines is hypothesized to contribute to an adaptive increase in cell wall flexibility and elasticity under cold stress. The enhanced flexibility may be particularly important in mitigating the effects of osmotic

stress, a major challenge faced by plants exposed to low temperatures.

Low temperatures can induce a cascade of physiological stresses in plants. One of the immediate consequences is the limitation of transpiration and disruption of water balance due to stomatal closure or reduced functionality under cold stress (Agurla *et al.*, 2018; Zeng *et al.*, 2024). Reduced transpiration, in turn, can hinder water uptake through the roots, contributing to osmotic stress. Furthermore, low temperatures can negatively impact cell membrane fluidity (Figures 4e and 5f), impairing water uptake and transport within the plant, and exacerbating osmotic imbalance (Wu *et al.*, 2023). Consequently, water efflux from the cell in response to osmotic stress causes protoplast shrinkage (Figure S1), leading to a loss of turgor pressure against the cell wall. The reduced internal pressure can cause the cell wall to buckle inward. While proline accumulation serves as a protective mechanism to maintain cell turgor and safeguard cellular components (Figures 4f and 5g), the enhanced cell wall flexibility and elasticity conferred by the *Bna-miR397a-BnaLAC2* module may offer an additional coping strategy against cold-induced osmotic stress. This adaptive response, involving modifications to cell wall properties, could explain the enrichment of pathways and other biological processes related to cell wall biosynthesis and remodelling observed in the DEG analysis of our transgenic lines.

Beyond the aforementioned responses, exposure to low temperatures triggers another cascade of events within plant cells, ultimately leading to the production of ROS (Wang *et al.*, 2024; Zhang *et al.*, 2022b). These molecules play a crucial role in the intricate response to chilling temperatures, acting as key signalling molecules that orchestrate the plant's adaptation. In particular, ROS activate pathways involved in antioxidant defence, osmotic adjustment, membrane modification and the production of cold-responsive protein (Castro *et al.*, 2021; Ding *et al.*, 2020). To counter oxidative damage, plants upregulate the production of antioxidant enzymes, including catalase (CAT), peroxidases (PER/POD) and glutathione S-transferase (GST), which scavenge excess ROS and mitigate downstream ROS-induced damage. Simultaneously, the activation of genes involved in the biosynthesis of osmoprotectants, helps maintain cell turgor under cold-induced dehydration. Furthermore, plants modify their cell membranes by increasing the proportion of unsaturated fatty acids, thereby maintaining fluidity at low temperatures. Notably, ROS could induce the structural switching and functional activation of cold-responsive C-repeat-binding transcription factors (CBFs), to facilitate plant adaptations to cold stress (Lee *et al.*, 2021; Wang *et al.*, 2024; Wi *et al.*, 2022). The miR397 is also found to be responsive to H₂O₂ stress in rice, and coordinate plants' responses under oxidative stress (Li *et al.*, 2011). Additionally, ROS can also function as signalling molecules that trigger lignin synthesis in plants. For instance, ROS induce the expression of key enzyme genes involved in lignin biosynthesis, such as phenylalanine ammonia-lyase (PAL), 4-coumarate-CoA ligase (4CL) and cinnamyl alcohol dehydrogenase (CAD), thereby promoting increased lignin accumulation (Liu *et al.*, 2024). Lignin biosynthesis, however, is an energy-intensive process. Therefore, the reduced lignin biosynthesis observed in *Bna-miR397a*OE and *Bnalac2* mutant lines likely conserves energy, enabling increased allocation towards bolstering ROS scavenging systems and other stress-resistance mechanisms. Conversely, sustained high levels of lignin biosynthesis in *Bna-STTM397a* line may deplete energy reserves, potentially compromising the efficiency of ROS scavenging. This hypothesis is supported by our observations: *Bna-*

STTM397a lines exhibited a notably weaker ROS scavenging system (Figure S12). While all tested CBF/COR genes that involving in osmotic adjustment displayed strong up-regulation at 21 DAC, their transcription was significantly decreased or only subtly altered in *Bna-STTM397a* lines plants (Figure S14).

There is evidence that a decrease in total lignin content is associated with enhanced cold stress (Jing *et al.*, 2023; Parrotta *et al.*, 2019). In *Arabidopsis*, lignin accumulation reduces the space available for ice crystal formation under freezing stress conditions, thereby compromising cell wall plasticity and increasing sensitivity to cold stress (Ji *et al.*, 2015). Transgenic switchgrass plants with reduced lignin content demonstrate enhanced cold tolerance (Liu *et al.*, 2017a). In maize, high levels of lignin have been found to impede cold acclimation during the early stages of cold stress but prove beneficial in later stages (Duran Garzon *et al.*, 2022). The relationship between lignin content and plant cold stress is complex and may depend on various factors, including plant species, developmental stage, tissue type and the duration of stress. Our study in *B. napus* suggests that the specific composition of lignin, particularly the S/G ratio mediated by the *Bna-miR397a-BnaLAC2* module plays a crucial role in conferring cold tolerance at the seedling stage. This finding adds a new layer of complexity to the understanding of lignin's role in plant cold stress response and highlights the importance of investigating lignin composition, beyond simply measuring total lignin content, when studying cold stress responses in plants. Further research is needed to understand how the *Bna-miR397a-BnaLAC2* module interacts with other cold stress response pathways and whether manipulating lignin composition can be used as a strategy to improve cold tolerance in other crop species.

Conclusion

This study presents the first comprehensive joint miRNAome and transcriptome analysis investigating miRNA-mediated pathways in the cold response of *B. napus*. Our work identifies 106 miRNA-mRNA modules potentially involved in cold adaptation and reveals *Bna-miR397a* as a positive regulator of this process. We demonstrate that *Bna-miR397a* targets and suppresses *BnaLAC2*, a laccase gene involved in lignin biosynthesis. Our findings strongly suggest that the *Bna-miR397a-BnaLAC2* module enhances cold adaptation by lignin remodelling, and ROS homeostasis. These findings provide valuable insights into miRNA-mediated regulatory networks and suggest new strategies for improving agronomic traits under long-term stress conditions. The datasets we generated for causal miRNAs and their target genes reveal the significant role these molecules play in cold adaptation. Future studies should focus on elucidating the specific mechanisms by which these miRNA-mRNA interactions confer cold tolerance and exploring the practical applications of these insights in *B. napus* breeding.

Experimental procedures

Plant materials

Two Chinese winter-type *B. napus* lines developed by Oil Crops Research Institute (Wuhan, China): the cold-tolerant 'C18' and cold-sensitive 'Zhongshuang 6' (C6), were used in this study (Yan *et al.*, 2018). The *Bna-miR397a* overexpressing lines have the genetic background of C6, while other transgenic lines generated in this study have the genetic background of *B. napus* cv. Westar.

Vector construction and transformation

To construct an overexpression vector of *Bna-miR397a*, a 228 bp DNA fragment including the predicted *Bna-miR397a* stem loop precursor was amplified from the *B. napus* cultivar C6 using miRNA specific primer pair *Bna-miR397a*-F/R and confirmed by sequencing. The fragment was then cloned into *EcoR* I/*Kpn* I sites of the vector pCambia1302 (Cambia; www.cambia.org).

To construct Short tandem target mimic (STTM) vector, the STTM backbone of *miR397a* was chemically synthesized (Tsingke Biological Technology, China) as described by (Tang et al., 2012), and ligated into binary vector PGTV-FLAG III.

To generate *BnaLAC2* CRISPR vector, specific guide RNAs targeted *BnaLAC2* (guide 1, TCTACATGCTAGCAAGACCT, guide 2, CCTATCAACAGTACGAGCTA) were designed by CRISPR-P (<http://crispr.hzau.edu.cn/CRISPR/>), and ligated to pYLCRISPR/Cas9-MH(B) vectors as previously reported (Ma et al., 2015).

All constructs were introduced into *Agrobacterium tumefaciens* strain GV3101 and subsequently transformed either into *B. napus* (C6/Westar) or *Arabidopsis* ecotype Columbia (Col-0) via *agrobacterium*-mediated transformation (Zhang et al., 2006; Zheng et al., 2020). All primers used were listed in Table S9.

Low temperature tolerance assay

Seeds from all lines were surface-sterilized for 10 min in a 30% bleach solution containing TWEEN20 (Sigma-Aldrich). Following sterilization, seeds were sown on 10 × 10 cm Petri dishes containing moistened filter paper and then cold-stratified in darkness at 4 °C for 7 days to promote uniform germination. Plants were initially grown under a 16-h photoperiod at 22 °C for 14 days, at which point most seedlings had reached the three-leaf stage. Seedlings were then transferred to a phytotron with a 16-h light (8 °C)/8-h dark (4 °C) cycle for 3 weeks to acclimate to cold stress conditions. Leaf samples were collected following cold stress, and seedling phenotypes were documented photographically. Fresh biomass was measured from six seedlings per line, with corresponding wild-type (WT) plants serving as controls. To assess freezing tolerance, separate cohort of 14-day-old seedlings was subjected to −4 °C for 3 h, followed by a 3-day recovery period under standard growth conditions (16-h light/8-h dark cycle at 22 °C). Survival rates were then measured. Each experimental line consisted of six pots containing four seedlings per pot. All measurements were performed in triplicate.

Determination of physiological indexes

The optical microscopic observation was performed as described in previous study with some modifications (Hajihashemi et al., 2018). The stem samples from *B. napus* seedlings were fixed in 50% formalin–acetic acid–alcohol (50% FAA 1:1:18 v/v) solution, and then dehydrated in ethanol and embedded in white resin. The stem cross-sections were stained with toluidine blue and observed using an optical microscope.

The electrolyte leakage (EL) was determined according to the previous method (Lv et al., 2016). Briefly, six completely expanded leaves from *Arabidopsis* or *B. napus* seedlings were sampled and divided into small discs about 0.5-inch diameter, and immediately transferred to a 50-mL test tube filled with 30-mL ddH₂O. After shaking overnight, the initial electric conductivity (EC1) was measured. The test tube with leaf discs was placed for 30 min in a boiling water bath and cooled down, the final electrical conductivity (EC2) was tested. The relative EL was calculated as the ratio of EC1 to EC2.

For each line, fresh biomass of aboveground part from 3 or more individual plants was obtained and subjected to statistical analyses. The proline content was investigated using the kits from Beijing Solarbio Science & Technology as described previously (Huang et al., 2020). Briefly, 0.2 g fresh tissue was powdered and incubated in 2 mL 3% sulfosalicylic acid. After centrifuging, 1 mL supernatant was mixed with corresponding reaction buffers and incubated at 95 °C in a water bath for 15 min, then the absorbance was measured using MULTISCAN FC (Thermo Scientific).

The ROS scavenging enzymes activity was measured by kits according to the manufacturer's instruction (Beijing Solarbio Science & Technology) with minor modification (Yan et al., 2019). 0.1 g fresh tissue was powdered using 1 mL 0.05 mol/L PBS buffer (PH 7.8). The supernatant was obtained after centrifuging at 12 000 *g* for 10 min at 4 °C, then was used for catalase (CAT) activity, peroxidase (POD) activity, superoxide dismutase (SOD) activity measurement. For glutathione S-transferase (GST) measurement, the supernatant was obtained after 0.1 g tissue powder incubating in 1 mL 0.05 mol/L PBS buffer (PH 6.8). For H₂O₂ measurement, 0.1 g fresh powder was incubated in 1 mL acetone. For MDA measurement, 0.2 g fresh powder was added 10% trichloroacetic acid (TCA). After centrifugation at 12 000 *g* for 10 min at 4 °C, the supernatant was mixed with 0.67% thiobarbituric acid (TBA) and boiled for 30 min. The absorbance was detected using MULTISCAN FC (Thermo Scientific).

The PSII effective photochemical quantum efficiency (Fv/Fm) was determined for fully expanded leaves with the chlorophyll fluorescence instrument (PAM-2500; Walz) after 30 min of dark adaptation. Data were recorded on five plants for each line with three readings per plant.

Chlorophyll from 0.1 g of rosette leaves was extracted with 1 mL 95% ethanol (v/v) after 12 h of dark incubation. The supernatant was obtained after centrifuging at 12 000 *g* for 10 min at 4 °C, and measured for chlorophyll assay at the absorbance at 665 and 649 nm using MULTISCAN FC (Thermo Scientific).

For DAB staining, leaves were incubated in 3, 3'-diaminobenzidine (DAB) (1 mg/mL, Sigma) for 12 h at room temperature without light, the stained leaves were observed after decolorizing in 75% alcohol several times.

Transient co-expression analysis

The isolation and transformation of *B. napus* protoplasts were performed according to a previously reported polyethylene glycol (PEG)-based method (Zheng et al., 2018). Briefly, the vectors were co-transformed into protoplasts according to the following combination: control transformations, empty vector (includes 35S only) plus 35S::BnaLAC2; experimental transformations, 35S::Bna-miR397a plus 35S::BnaLAC2/BnaLAC4-1/BnaLAC4-2/BnaLAC17. After overnight incubation at 25 °C, the protoplasts were collected in 600 µL Trizol reagent (Invitrogen) and RNA was extracted. 1 µg RNA was transcribed to first-strand cDNA; the relative expression levels of *Bna-miR397a*, and candidate target genes were analysed following the quantitative real-time PCR (qRT-PCR) method (Wang et al., 2014b).

For dual-LUC assays, the CDs sequence of BnaLAC2 was inserted into optimized pGreenII 0800-LUC, which was used as Reporter. *Bna-miR397a* precursor was inserted into pGreenII 62-SK effector vectors, which was used as Effector. The empty vector pGreenII 62-SK was used as control (CK). The *Agrobacterium*-mediated transient transformation was applied on leaves of 4-

week-old tobacco (*N. benthamiana*) plants as previously described (Zhang *et al.*, 2020). The LUC activity was measured using the Dual-Luciferase Reporter Assay System (Promega) on GLOMAX luminometer (Promega).

Identification of cleavage site of *Bna-miR397a*

The mRNA was purified from total RNA using PolyATtract® mRNA isolation system (Promega) following manufacturer instructions. The cleavage sites of *BnaLAC2* targeted by *Bna-miR397a* in *B. napus* were determined using RNA ligase-mediated rapid amplification of cDNA ends (RLM-RACE) (Khandal *et al.*, 2020). First choice® 5'-RLM-RACE kit (Invitrogen) was used according to the manufacturer's protocol. RNA oligo adapter was ligated at 5'-end of mRNA and reverse transcribed by SuperScript III RT using oligo DT primers to synthesize cDNA. In first PCR, cDNA was amplified with 5' adapter specific primer (ASP) and 3' gene-specific primer (GSP) 1. First PCR product was used as a template in nested PCR by using ASP and GSP2 primers. The final product was gel purified, TA cloned and sequenced using M13 sequencing primers to obtain the specific site of miRNA cleavage. RACE and the gene-specific primers were listed in Table S9.

RNA extraction, library preparation and transcriptome sequencing

The leaves of *B. napus* seedlings were sampled before 0 day (C18-0, C6-0), and after 1 day (C18-1, C6-1), 7 days (C18-7, C6-7), 14 days (C18-14, C6-14), 21 days (C18-21, C6-21) cold stress treatment based on three biological replications. For *Bna-miR397a* and *Bnalac2* related RNA-seq, the seedling leaves from *Bna-miR397aOE1*, *Bna-miR397aOE2*, *Bna-miR397aOE3*, ZS6, *Bna-STTM397a-1*, *Bna-STTM397a-2*, *Bna-STTM397a-3*, Westar, *Bnalac2-1*, *Bnalac2-2* were sampled after 21 days cold treatment based on three biological replications. All the samples were flash-frozen in liquid nitrogen and stored in -80°C until use. RNA was isolated using TRIzol Reagent (Invitrogen). The RNA integrity and purity were quantified using RNA Nano 6000 Assay Kit of the Agilent Bioanalyzer 2100 system. Sequencing libraries were generated using the NEBNext Ultra™ RNA Library Prep Kit for Illumina (NEB, Ipswich, MA). Briefly, mRNA was purified from total RNA using poly(dT) oligo-linked magnetic beads. First-strand and second-strand cDNAs were synthesized. NEBNext Adaptor with a hairpin loop structure was ligated to DNA fragments for hybridization after adenylation of their 3' ends. The library fragments were purified using the AMPure XP system (Beckman Coulter, Beverly, MA). The USER Enzyme (NEB) was added to the cDNA at 37°C for 15 min, followed by 5 min at 95°C before the PCR process. The PCR reaction was performed using Phusion High-Fidelity DNA polymerase, universal PCR primers and index primers. Finally, the PCR products were purified with AMPure XP system and the library quality was evaluated using the Agilent Bioanalyzer 2100 system. The RNA-seq was performed using the Illumina HiSeq x-ten platform and paired-end reads were generated at Beijing Biomarker Technologies Co. Ltd. (Beijing, China). Clean reads were obtained from raw reads based on quality score, length and N content using the in-house perl-scripts. Q20, Q30, GC-content and sequence duplication levels of the clean data were measured. The adaptor sequences and the low-quality regions of raw reads were clipped with Trimmomatic (Bolger *et al.*, 2014). The HISAT2 v2.1.0 software was used to map high-quality, unique reads to the reference genome of *B. napus* (<http://www.genoscope.cns.fr/brassicanapus/>) (Chalhoub *et al.*, 2014). The average gene expression, in uniquely

mapped reads, was measured by Fragments Per Kilobase exon Model (FPKM) per Million mapped reads. Differential expression analysis of genes in designed comparisons was measured using DESeq2 software. The resulting *P* values were adjusted using the Benjamini and Hochberg's method to control the false discovery rate (FDR). Genes with absolute $\log_2\text{FC} \geq 2$ or ≤ -2 , adjusted $P < 0.001$, and FDR < 0.001 were declared as differentially expressed.

The above *B. napus* samples of C18 and C6 were also prepared for small RNA quantification and qualification. All sequencing procedures were performed by the BioMarker Technologies Company Beijing, China (www.biomarker.com.cn). For small RNA library preparation, the 3' SR and 5' SR adaptors were ligated, followed by reverse transcription to synthesize the first chain. PCR amplification was performed using LongAmp Taq 2 × Master Mix with SR primer for Illumina and index (X) primer. The PCR products were purified using the AMPure XP system and assessed using TruSeq PE Cluster Kit (Illumina) following the manufacturer's instructions. The high-quality libraries were sequenced on an Illumina platform. To analyse sRNA-seq data, the clean sequence reads were processed using miRDeep2 and aligned to miRBase 22.0 (<http://www.mirbase.org>) to identify the novel and known miRNAs expressed in *B. napus*. The DESeq2 R package (1.10.1) was used for differential expression analysis of miRNA. The threshold selection criteria $\log_2|\text{FC}| \geq 0.584$ (Harrop *et al.*, 2019), and *P*-value adjusted based on *q* value, was applied to filter out DEMs. The raw data of the RNA-seq and sRNA-seq of C18 and C6 was submitted to NCBI SRA database with accession number PRJNA596550, followed by SUB14607625 of *Bna-miR397a* and *Bnalac2* related RNA-seq data.

Bioinformatics analysis

Differentially expressed genes were assigned Gene Ontology (GO) terms by the Goseq R packages based Wallenius non-central hyper-geometric distribution. KOBAS software was used to assign the Kyoto Encyclopedia of Genes and Genomes (KEGG) pathways (<http://www.genome.jp/kegg/>) for DEGs (Mao *et al.*, 2005). Target genes were predicted using the online web tool PSRNAT (<http://plantgrn.noble.org/psRNATarget/>) (Dai *et al.*, 2018). DEGs, DEMs and target DEGs were clustered by Genesis (version 1.7.7). K-means clustering was performed based on $\log_2\text{FPKM}$ in C6 and C18 using Inertia and Elbow Method (Sturn *et al.*, 2002). The number of clusters was manually selected keeping in view following assumptions: the data points assigned to specific cluster remain the same; centroids remain the same; the distance of data points from their centroid is minimum. Circos diagram was visualized using Circos (Kim *et al.*, 2014).

To identify conserved and novel miRNAs in *B. napus*, 413.14 million (M) high-quality reads (average Q20 > 99% and Q30 > 98%) were analysed using miRDeep2 and compared against miRBase 22.0 (<http://www.mirbase.org>).

Quantitative real-time PCR (qRT-PCR)

Samples were flash-frozen in liquid nitrogen and stored in -80°C until use. RNA was isolated using TRIzol Reagent (Invitrogen) and 2 μg of total RNA was converted into cDNA using EasyScript® One-Step cDNA Synthesis SuperMix (Trans) following the manufacturer's instructions. qRT-PCR was performed using the primers listed in Table S9. For Stem-loop (SL) qRT-PCR, primer designed for miRNA reverse transcription harbours the last six bases of mature miRNA at 3' end, while primer designed from the backbone of SL was used as a universal

reverse primer. *U6* and *BnaACTIN* were used as internal control for miRNA and genes, respectively. qRT-PCR reactions were performed on StepOnePlusReal-Time PCR System (Applied Biosystems) using the SYBR®Green PCR Master Mix (Applied Biosystems) reaction mix (10 µL). The results were analysed using $2^{-\Delta\Delta CT}$ method (Wang *et al.*, 2014b) in three biological triplicates.

Lignin analysis

The lignin includes acid-insoluble and -soluble lignin. The acid-insoluble lignin was calculated gravimetrically as acid-insoluble residue after correction for ash, the acid-soluble lignin was solubilized during the hydrolysis process, and was measured by UV spectroscopy. The total lignin content was calculated by the sum of the acid-insoluble and soluble lignin contents according to previous method (Wu *et al.*, 2013). The lignin monomer composition was determined by HPLC as previously described (Xu *et al.*, 2012). Briefly, the standard chemicals that including p-Hydroxybenzaldehyde (H), vanillin (G) and syringaldehyde (S) were purchased from Sinopharm Chemical Reagent Co., Ltd. The sample was extracted with benzene-ethanol (2:1, v/v) in a Soxhlet for 4 h, the remaining pellet was collected as cell wall residue. After the procedure of nitrobenzene oxidation of cell wall residue, the oxidation products were dissolved in chromatographic pure methanol and analysed by HPLC with a UV-detector at 280 nm.

For histochemical analysis, phloroglucinol-HCl staining was performed according to the previous method (Weng *et al.*, 2010). Stem of *B. napus* plants were sampled before and after 21 days of cold treatment with FAA fixative solution (45% ethanol, 6% acetic acid, 5% formaldehyde), then stained with 1% phloroglucinol (w/v) in 12% HCl for 5 min and immediately observed with a light microscope.

Statistical analysis

Excel (2007) and SPSS (22.0) software were used for statistical analysis. Two-way ANOVA was calculated to find the significant differences between the effect of genotypes and the respective treatments. For Student's *t*-test, $P < 0.05$ and $P < 0.01$ were considered statistically significant (*) and highly significant (**), respectively. Statistix 8.1 was used for the Tukey–Kramer test for pairwise comparison.

Acknowledgements

We thank Professor Y. Zhou of the Institute of Genetics and Developmental Biology, Chinese Academy of Sciences, for insightful discussions on cell wall characteristics. This work is supported by grants from the National Key Research and Development Program of China (2023YFF1000700), the National Natural Science Foundation of China (32470302, 32300268), Sci-Tech Innovation 2030 Agenda (2022ZD04009), the Natural Science Foundation of Jiangsu Higher Education Institutions of China (23KJA210002), the Hubei Provincial Agricultural Science and Technology Innovation Center Innovation Team (2021-620-000-001-035), the Priority Academic Program Development of Jiangsu Higher Education Institutions (PAPD), Open Funding Project of the State Key Laboratory of Biocatalysis and Enzyme Engineering (SKLBEE2020012), the Key Research Program & Technology Innovation Program of Chinese Academy of Agricultural Sciences (CAAS-ZDRW202105). The open funds of the Key Laboratory of Plant Functional Genomics of the Ministry of Education (ML202403).

Conflict of interest

The authors have declared no conflict of interest.

Author contributions

Y.L. and K.H. conceived and supervised the study, designed some of the experiments, interpreted data and revised the manuscript. M.A.H. and Y.H. designed and performed most experiments, analysed the data and drafted the manuscript with input from D.L., S.S.M., X.Z., Y.C., L.Z., X.D., X.Z., B.W., L.D., B.W. and A.R. All authors reviewed and approved the submitted version.

Consent for publication

All authors consent for publication.

Data availability statement

All data generated in the present study are included in this published article and in additional information. The raw data of the RNA-seq and sRNA-seq was submitted to NCBI SRA database with accession number PRJNA596550.

References

- Agurla, S., Gahir, S., Munemasa, S., Murata, Y. and Raghavendra, A.S. (2018) Mechanism of stomatal closure in plants exposed to drought and cold stress. *Adv. Exp. Med. Biol.* **1081**, 215–232.
- Ahmed, S., Rashid, M.A.R., Zafar, S.A., Azhar, M.T., Waqas, M., Uzair, M., Rana, I.A. *et al.* (2021) Genome-wide investigation and expression analysis of APETALA-2 transcription factor subfamily reveals its evolution, expansion and regulatory role in abiotic stress responses in Indica Rice (*Oryza sativa* L. ssp. *indica*). *Genomics*, **113**, 1029–1043.
- Aydinoglu, F. (2020) Elucidating the regulatory roles of microRNAs in maize (*Zea mays* L.) leaf growth response to chilling stress. *Planta*, **251**, 38.
- Barros, J., Escamilla-Trevino, L., Song, L., Rao, X., Serrani-Yarce, J.C., Palacios, M.D., Engle, N. *et al.* (2019) 4-coumarate 3-hydroxylase in the lignin biosynthesis pathway is a cytosolic ascorbate peroxidase. *Nat. Commun.* **10**, 1994.
- Beauchair, L., Yu, A. and Bouché, N. (2010) microRNA-directed cleavage and translational repression of the copper chaperone for superoxide dismutase mRNA in *Arabidopsis*. *Plant J.* **62**, 454–462.
- Bolger, A.M., Lohse, M. and Usadel, B. (2014) Trimmomatic: a flexible trimmer for Illumina sequence data. *Bioinformatics*, **30**, 2114–2120.
- Campos, P.S., Quartin, V., Ramalho, J.C. and Nunes, M.A. (2003) Electrolyte leakage and lipid degradation account for cold sensitivity in leaves of *Coffea* sp. plants. *J. Plant Physiol.* **160**, 283–292.
- Castro, B., Citterico, M., Kimura, S., Stevens, D.M., Wrzaczek, M. and Coaker, G. (2021) Stress-induced reactive oxygen species compartmentalization, perception and signalling. *Nat. Plants*, **7**, 403–412.
- Chalhoub, B., Denoeud, F., Liu, S., Parkin, I.A., Tang, H., Wang, X., Chiquet, J. *et al.* (2014) Plant genetics. Early allopolyploid evolution in the post-Neolithic *Brassica napus* oilseed genome. *Science*, **345**, 950–953.
- Chen, L., Zhong, H., Ren, F., Guo, Q.Q., Hu, X.P. and Li, X.B. (2011) A novel cold-regulated gene, COR25, of *Brassica napus* is involved in plant response and tolerance to cold stress. *Plant Cell Rep.* **30**, 463–471.
- Chen, H., Chen, X., Chai, X., Qiu, Y., Gong, C., Zhang, Z., Wang, T. *et al.* (2015) Effects of low temperature on mRNA and small RNA transcriptomes in *Solanum lycopersicoides* leaf revealed by RNA-Seq. *Biochem. Biophys. Res. Commun.* **464**, 768–773.
- Dahal, K., Gadapati, W., Savitch, L.V., Singh, J. and Hüner, N.P. (2012) Cold acclimation and BnCBF17-over-expression enhance photosynthetic

- performance and energy conversion efficiency during long-term growth of *Brassica napus* under elevated CO₂ conditions. *Planta*, **236**, 1639–1652.
- Dai, X., Zhuang, Z. and Zhao, P.X. (2018) psRNATarget: a plant small RNA target analysis server (2017 release). *Nucleic Acids Res.* **46**, W49–W54.
- Ding, Y. and Yang, S. (2022) Surviving and thriving: how plants perceive and respond to temperature stress. *Dev. Cell*, **57**, 947–958.
- Ding, Y., Lv, J., Shi, Y., Gao, J., Hua, J., Song, C., Gong, Z. *et al.* (2019) EGR2 phosphatase regulates OST1 kinase activity and freezing tolerance in *Arabidopsis*. *EMBO J.* **38**, e99819.
- Ding, Y., Shi, Y. and Yang, S. (2020) Molecular regulation of plant responses to environmental temperatures. *Mol. Plant*, **13**, 544–564.
- Dong, C. and Pei, H. (2014) Over-expression of miR397 improves plant tolerance to cold stress in *Arabidopsis thaliana*. *J. Plant Biol.* **57**, 209–217.
- Duran Garzon, C., Lequart, M., Charras, Q., Fournet, F., Bellenger, L., Sellier-Richard, H., Giauffret, C. *et al.* (2022) The maize low-lignin brown midrib3 mutant shows pleiotropic effects on photosynthetic and cell wall metabolisms in response to chilling. *Plant Physiol. Biochem.* **184**, 75–86.
- Fang, C., Zhang, P., Jian, X., Chen, W., Lin, H., Li, Y. and Lin, W. (2017) Overexpression of Lsi1 in cold-sensitive rice mediates transcriptional regulatory networks and enhances resistance to chilling stress. *Plant Sci.* **262**, 115–126.
- Gaddam, S.R., Sharma, A. and Trivedi, P.K. (2024) miR397b-LAC2 module regulates cadmium stress response by coordinating root lignification and copper homeostasis in *Arabidopsis thaliana*. *J. Hazard. Mater.* **465**, 133100.
- Guo, D., Chen, F., Inoue, K., Blount, J.W. and Dixon, R.A. (2001) Downregulation of caffeic acid 3-O-methyltransferase and caffeoyl CoA 3-O-methyltransferase in transgenic alfalfa: impacts on lignin structure and implications for the biosynthesis of G and S lignin. *Plant Cell*, **13**, 73–88.
- Guo, H.S., Xie, Q., Fei, J.F. and Chua, N.H. (2005) MicroRNA directs mRNA cleavage of the transcription factor NAC1 to downregulate auxin signals for *Arabidopsis* lateral root development. *Plant Cell*, **17**, 1376–1386.
- Guo, Y., Wang, S., Yu, K., Wang, H., Xu, H., Song, C., Zhao, Y. *et al.* (2023) Manipulating microRNA miR408 enhances both biomass yield and saccharification efficiency in poplar. *Nat. Commun.* **14**, 4285.
- Gupta, O.P., Meena, N.L., Sharma, I. and Sharma, P. (2014) Differential regulation of microRNAs in response to osmotic, salt and cold stresses in wheat. *Mol. Biol. Rep.* **41**, 4623–4629.
- Hajhashemi, S., Noedoost, F., Geuns, J.M.C., Djalic, I. and Siddique, K.H.M. (2018) Effect of cold stress on photosynthetic traits, carbohydrates, morphology, and anatomy in nine cultivars of *Stevia rebaudiana*. *Front. Plant Sci.* **9**, 1430.
- Harrop, T.W.R., Mantegazza, O., Luong, A.M., Béthune, K., Lorieux, M., Jouannic, S. and Adam, H. (2019) A set of AP2-like genes is associated with inflorescence branching and architecture in domesticated rice. *J. Exp. Bot.* **70**, 5617–5629.
- Huang, Y., Hussain, M.A., Luo, D., Xu, H., Zeng, C., Havlickova, L., Bancroft, I. *et al.* (2020) A *Brassica napus* reductase gene dissected by associative transcriptomics enhances plant adaption to freezing stress. *Front. Plant Sci.* **11**, 971.
- Huo, C., Zhang, B. and Wang, R. (2022) Research progress on plant noncoding RNAs in response to low-temperature stress. *Plant Signal. Behav.* **17**, 2004035.
- Ji, H., Wang, Y., Cloix, C., Li, K., Jenkins, G.I., Wang, S., Shang, Z. *et al.* (2015) The *Arabidopsis* RCC1 family protein TCF1 regulates freezing tolerance and cold acclimation through modulating lignin biosynthesis. *PLoS Genet.* **11**, e1005471.
- Jiang, B., Shi, Y., Zhang, X., Xin, X., Qi, L., Guo, H., Li, J. *et al.* (2017) PIF3 is a negative regulator of the CBF pathway and freezing tolerance in *Arabidopsis*. *Proc. Natl. Acad. Sci. USA*, **114**, E6695–E6702.
- Jing, Y., Pei, T., Li, C., Wang, D., Wang, Q., Chen, Y., Li, P. *et al.* (2023) Overexpression of the FERONIA receptor kinase MdMLK2 enhances apple cold tolerance. *Plant J.* **115**, 236–252.
- Ke, L., Lei, W., Yang, W., Wang, J., Gao, J., Cheng, J., Sun, Y. *et al.* (2020) Genome-wide identification of cold responsive transcription factors in *Brassica napus* L. *BMC Plant Biol.* **20**, 62.
- Khandal, H., Singh, A.P. and Chattopadhyay, D. (2020) The MicroRNA397b-LACCASE2 module regulates root lignification under water and phosphate deficiency. *Plant Physiol.* **182**, 1387–1403.
- Kidokoro, S., Yoneda, K., Takasaki, H., Takahashi, F., Shinozaki, K. and Yamaguchi-Shinozaki, K. (2017) Different cold-signaling pathways function in the responses to rapid and gradual decreases in temperature. *Plant Cell*, **29**, 760–774.
- Kim, C.K., Lim, H.M., Na, J.K., Choi, J.W., Sohn, S.H., Park, S.C., Kim, Y.H. *et al.* (2014) A multistep screening method to identify genes using evolutionary transcriptome of plants. *Evol. Bioinform. Online*, **10**, 69–78.
- Kumar, S. and Trivedi, P.K. (2018) Glutathione S-transferases: role in combating abiotic stresses including arsenic detoxification in plants. *Front. Plant Sci.* **9**, 751.
- Kutsuno, T., Chowhan, S., Kotake, T. and Takahashi, D. (2023) Temporal cell wall changes during cold acclimation and deacclimation and their potential involvement in freezing tolerance and growth. *Physiol. Plant.* **175**, e13837.
- Lee, E.S., Park, J.H., Wi, S.D., Kang, C.H., Chi, Y.H., Chae, H.B., Paeng, S.K. *et al.* (2021) Redox-dependent structural switch and CBF activation confer freezing tolerance in plants. *Nat. Plants*, **7**, 914–922.
- Leplé, J.C., Dauwe, R., Morreel, K., Storme, V., Lapierre, C., Pollet, B., Naumann, A. *et al.* (2007) Downregulation of cinnamoyl-coenzyme A reductase in poplar: multiple-level phenotyping reveals effects on cell wall polymer metabolism and structure. *Plant Cell*, **19**, 3669–3691.
- Li, T., Li, H., Zhang, Y.X. and Liu, J.Y. (2011) Identification and analysis of seven H₂O₂-responsive miRNAs and 32 new miRNAs in the seedlings of rice (*Oryza sativa* L. ssp. *indica*). *Nucleic Acids Res.* **39**, 2821–2833.
- Li, J., Guo, G., Guo, W., Guo, G., Tong, D., Ni, Z., Sun, Q. *et al.* (2012) miRNA164-directed cleavage of ZmNAC1 confers lateral root development in maize (*Zea mays* L.). *BMC Plant Biol.* **12**, 220.
- Li, A., Li, G., Zhao, Y., Meng, Z., Zhao, M., Li, C., Zhang, Y. *et al.* (2018) Combined small RNA and gene expression analysis revealed roles of miRNAs in maize response to rice black-streaked dwarf virus infection. *Sci. Rep.* **8**, 13502.
- Liu, Y., Wang, K., Li, D., Yan, J. and Zhang, W. (2017a) Enhanced cold tolerance and tillering in switchgrass (*Panicum virgatum* L.) by heterologous expression of Osa-miR393a. *Plant Cell Physiol.* **58**, 2226–2240.
- Liu, Z., Jia, Y., Ding, Y., Shi, Y., Li, Z., Guo, Y., Gong, Z. *et al.* (2017b) Plasma membrane CRPK1-mediated phosphorylation of 14-3-3 proteins induces their nuclear import to fine-tune CBF signaling during cold response. *Mol. Cell*, **66**, 117–128.e115.
- Liu, C., Feng, Z.C., Xiao, T.H., Ma, X.M., Zhou, G.S. and Huang, F.H. (2019) Development, potential and adaption of Chinese rapeseed industry. *Chinese J. Oil Crop Sci.* **41**, 485–489.
- Liu, L., Chen, Y., Wu, W., Chen, Q., Tian, Z., Huang, J., Ren, H. *et al.* (2024) A multilevel investigation to reveal the regulatory mechanism of lignin accumulation in juice sac granulation of pomelo. *BMC Plant Biol.* **24**, 390.
- Lu, X., Dun, H., Lian, C., Zhang, X., Yin, W. and Xia, X. (2017) The role of peu-miR164 and its target PeNAC genes in response to abiotic stress in *Populus euphratica*. *Plant Physiol. Biochem.* **115**, 418–438.
- Lu, Q., Guo, F., Xu, Q. and Cang, J. (2020) lncRNA improves cold resistance of winter wheat by interacting with miR398. *Funct. Plant Biol.* **47**, 544–557.
- Luo, T., Xian, M., Zhang, C., Zhang, C., Hu, L. and Xu, Z. (2019) Associating transcriptional regulation for rapid germination of rapeseed (*Brassica napus* L.) under low temperature stress through weighted gene co-expression network analysis. *Sci. Rep.* **9**, 55.
- Lv, Y., Guo, Z., Li, X., Ye, H., Li, X. and Xiong, L. (2016) New insights into the genetic basis of natural chilling and cold shock tolerance in rice by genome-wide association analysis. *Plant Cell Environ.* **39**, 556–570.
- Ma, X., Zhang, Q., Zhu, Q., Liu, W., Chen, Y., Qiu, R., Wang, B. *et al.* (2015) A robust CRISPR/Cas9 system for convenient, high-efficiency multiplex genome editing in monocot and dicot plants. *Mol. Plant*, **8**, 1274–1284.
- Mao, X., Cai, T., Olyarchuk, J.G. and Wei, L. (2005) Automated genome annotation and pathway identification using the KEGG Orthology (KO) as a controlled vocabulary. *Bioinformatics*, **21**, 3787–3793.
- Megha, S., Basu, U., Joshi, R.K. and Kav, N.N.V. (2018) Physiological studies and genome-wide microRNA profiling of cold-stressed *Brassica napus*. *Plant Physiol. Biochem.* **132**, 1–17.
- Orvar, B.L., Sangwan, V., Omann, F. and Dhindsa, R.S. (2000) Early steps in cold sensing by plant cells: the role of actin cytoskeleton and membrane fluidity. *Plant J.* **23**, 785–794.
- Parrotta, L., Falieri, C., Guerriero, G. and Cai, G. (2019) Cold stress affects cell wall deposition and growth pattern in tobacco pollen tubes. *Plant Sci.* **283**, 329–342.

- Pu, Y., Liu, L., Wu, J., Zhao, Y., Bai, J., Ma, L., Yue, J. et al. (2019) Transcriptome profile analysis of winter rapeseed (*Brassica napus* L.) in response to freezing stress, reveal potentially connected events to freezing stress. *Int. J. Mol. Sci.* **20**, 1–24.
- Qi, G., Chen, H., Wang, D., Zheng, H., Tang, X., Guo, Z., Cheng, J. et al. (2021) The BZR1-EDS1 module regulates plant growth-defense coordination. *Mol. Plant*, **14**, 2072–2087.
- Quan, M., Du, Q., Xiao, L., Lu, W., Wang, L., Xie, J., Song, Y. et al. (2019) Genetic architecture underlying the lignin biosynthesis pathway involves noncoding RNAs and transcription factors for growth and wood properties in *Populus*. *Plant Biotechnol. J.* **17**, 302–315.
- Savitch, L.V., Allard, G., Seki, M., Robert, L.S., Tinker, N.A., Huner, N.P., Shinozaki, K. et al. (2005) The effect of overexpression of two *Brassica* CBF/DREB1-like transcription factors on photosynthetic capacity and freezing tolerance in *Brassica napus*. *Plant Cell Physiol.* **46**, 1525–1539.
- Shen, X., Song, Y., Ping, Y., He, J., Xie, Y., Ma, F., Li, X. et al. (2023) The RNA-binding protein MdHYL1 modulates cold tolerance and disease resistance in apple. *Plant Physiol.* **192**, 2143–2160.
- Shi, Y., Ding, Y. and Yang, S. (2018) Molecular regulation of CBF signaling in cold acclimation. *Trends Plant Sci.* **23**, 623–637.
- Song, J.B., Gao, S., Sun, D., Li, H., Shu, X.X. and Yang, Z.M. (2013) miR394 and LCR are involved in *Arabidopsis* salt and drought stress responses in an abscisic acid-dependent manner. *BMC Plant Biol.* **13**, 210.
- Song, J.B., Gao, S., Wang, Y., Li, B.W., Zhang, Y.L. and Yang, Z.M. (2016) miR394 and its target gene LCR are involved in cold stress response in *Arabidopsis*. *Plant Gene*, **5**, 56–64.
- Song, G., Zhang, R., Zhang, S., Li, Y., Gao, J., Han, X., Chen, M. et al. (2017) Response of microRNAs to cold treatment in the young spikes of common wheat. *BMC Genomics*, **18**, 212.
- Sturn, A., Quackenbush, J. and Trajanoski, Z. (2002) Genesis: cluster analysis of microarray data. *Bioinformatics*, **18**, 207–208.
- Sunkar, R. and Zhu, J.K. (2004) Novel and stress-regulated microRNAs and other small RNAs from *Arabidopsis*. *Plant Cell*, **16**, 2001–2019.
- Tang, J. and Chu, C. (2017) MicroRNAs in crop improvement: fine-tuners for complex traits. *Nat. Plants*, **3**, 17077.
- Tang, G., Yan, J., Gu, Y., Qiao, M., Fan, R., Mao, Y. and Tang, X. (2012) Construction of short tandem target mimic (STTM) to block the functions of plant and animal microRNAs. *Methods*, **58**, 118–125.
- Tenhaken, R. (2014) Cell wall remodeling under abiotic stress. *Front. Plant Sci.* **5**, 771.
- Thomashow, M.F. (2010) Molecular basis of plant cold acclimation: insights gained from studying the CBF cold response pathway. *Plant Physiol.* **154**, 571–577.
- Wang, H.-Z. (2018) New-demand oriented oilseed rape industry developing strategy. *Chinese J. Oil Crop Sci.* **40**, 613–617.
- Wang, C.Y., Zhang, S., Yu, Y., Luo, Y.C., Liu, Q., Ju, C., Zhang, Y.C. et al. (2014a) MiR397b regulates both lignin content and seed number in *Arabidopsis* via modulating a laccase involved in lignin biosynthesis. *Plant Biotechnol. J.* **12**, 1132–1142.
- Wang, Z., Chen, Y., Fang, H., Shi, H., Chen, K., Zhang, Z. and Tan, X. (2014b) Selection of reference genes for quantitative reverse-transcription polymerase chain reaction normalization in *Brassica napus* under various stress conditions. *Mol. Gen. Genomics*, **289**, 1023–1035.
- Wang, X., Liu, S., Sun, H., Liu, C., Li, X., Liu, Y., Deguo, L. et al. (2021) Production of reactive oxygen species by PuRBOHF is critical for stone cell development in pear fruit. *Hortic. Res.* **8**, 249.
- Wang, P., Liu, W.C., Han, C., Wang, S., Bai, M.Y. and Song, C.P. (2024) Reactive oxygen species: multidimensional regulators of plant adaptation to abiotic stress and development. *J. Integr. Plant Biol.* **66**, 330–367.
- Weng, J.K., Akiyama, T., Bonawitz, N.D., Li, X., Ralph, J. and Chapple, C. (2010) Convergent evolution of syringyl lignin biosynthesis via distinct pathways in the lycophyte *Selaginella* and flowering plants. *Plant Cell*, **22**, 1033–1045.
- Wi, S.D., Lee, E.S., Park, J.H., Chae, H.B., Paeng, S.K., Bae, S.B., Phan, T.K.A. et al. (2022) Redox-mediated structural and functional switching of C-repeat binding factors enhances plant cold tolerance. *New Phytol.* **233**, 1067–1073.
- Woo, H.R., Koo, H.J., Kim, J., Jeong, H., Yang, J.O., Lee, I.H., Jun, J.H. et al. (2016) Programming of plant leaf senescence with temporal and inter-organellar coordination of transcriptome in *Arabidopsis*. *Plant Physiol.* **171**, 452–467.
- Wu, Z., Zhang, M., Wang, L., Tu, Y., Zhang, J., Xie, G., Zou, W. et al. (2013) Biomass digestibility is predominantly affected by three factors of wall polymer features distinctive in wheat accessions and rice mutants. *Biotechnol. Biofuels*, **6**, 183.
- Wu, G., Baumeister, R. and Heimbucher, T. (2023) Molecular mechanisms of lipid-based metabolic adaptation strategies in response to cold. *Cells*, **12**, 1353.
- Xiao, Z.L., Pan, Y.Y., Wang, C., Li, X.C., Lu, Y.Q., Tian, Z., Kuang, L.Q. et al. (2022) Multi-functional development and utilization of rapeseed: comprehensive analysis of the nutritional value of rapeseed sprouts. *Foods*, **11**, 778.
- Xu, N., Zhang, W., Ren, S., Liu, F., Zhao, C., Liao, H., Xu, Z. et al. (2012) Hemicelluloses negatively affect lignocellulose crystallinity for high biomass digestibility under NaOH and H₂SO₄ pretreatments in *Miscanthus*. *Biotechnol. Biofuels*, **5**, 58.
- Xue, C., Yao, J.L., Qin, M.F., Zhang, M.Y., Allan, A.C., Wang, D.F. and Wu, J. (2019) PbmiR397a regulates lignification during stone cell development in pear fruit. *Plant Biotechnol. J.* **17**, 103–117.
- Yan, L., Cai, J.S., Gao, L.B., Huang, B., Ma, H.Q., Liu, Q.Y., Dai, X.Y. et al. (2018) Identification method and selection of cold tolerance in rapeseed (*Brassica napus* L.). *Chinese J. Oil Crop Sci.* **40**, 74.
- Yan, L., Shah, T., Cheng, Y., Lv, Y., Zhang, X. and Zou, X. (2019) Physiological and molecular responses to cold stress in rapeseed (*Brassica napus* L.). *J. Integr. Agric.* **18**, 2742–2752.
- Yang, S. (2022) Cold responses in rice: From physiology to molecular biology. *J. Plant Physiol.* **269**, 153602.
- Yang, C., Li, D., Mao, D., Liu, X., Ji, C., Li, X., Zhao, X. et al. (2013) Overexpression of microRNA319 impacts leaf morphogenesis and leads to enhanced cold tolerance in rice (*Oryza sativa* L.). *Plant Cell Environ.* **36**, 2207–2218.
- Yu, Y., He, R.R., Yang, L., Feng, Y.Z., Xue, J., Liu, Q., Zhou, Y.F. et al. (2024) A transthyretin-like protein acts downstream of miR397 and LACCASE to regulate grain yield in rice. *Plant Cell*, **147**, 2893–2907.
- Zeng, R., Zhang, X., Song, G., Lv, Q., Li, M., Fu, D., Zhang, Z. et al. (2024) Genetic variation in the aquaporin TONOLAST INTRINSIC PROTEIN 4;3 modulates maize cold tolerance. *Plant Biotechnol. J.* **22**, 3037–3050.
- Zhang, X., Henriques, R., Lin, S.S., Niu, Q.W. and Chua, N.H. (2006) Agrobacterium-mediated transformation of *Arabidopsis thaliana* using the floral dip method. *Nat. Protoc.* **1**, 641–646.
- Zhang, Y.C., Yu, Y., Wang, C.Y., Li, Z.Y., Liu, Q., Xu, J., Liao, J.Y. et al. (2013) Overexpression of microRNA OsmiR397 improves rice yield by increasing grain size and promoting panicle branching. *Nat. Biotechnol.* **31**, 848–852.
- Zhang, B., Yang, H.J., Yang, Y.Z., Zhu, Z.Z., Li, Y.N., Qu, D. and Zhao, Z.Y. (2020) mdm-miR828 participates in the feedback loop to regulate anthocyanin accumulation in apple peel. *Front. Plant Sci.* **11**, 608109.
- Zhang, C., Chang, W., Li, X., Yang, B., Zhang, L., Xiao, Z., Li, J. et al. (2022a) Transcriptome and small RNA sequencing reveal the mechanisms regulating harvest index in *Brassica napus*. *Front. Plant Sci.* **13**, 855486.
- Zhang, H., Zhu, J., Gong, Z. and Zhu, J. (2022b) Abiotic stress responses in plants. *Nat. Rev. Genet.* **23**, 104–119.
- Zheng, M., Yang, H., Tang, M., Liu, J., Li, X. and Zhang, L. (2018) Cotyledons: a useful biological material for transient gene expression analysis in rapeseed (*Brassica napus* L.). *Oil Crop Sci.* **3**, 1–9.
- Zheng, M., Zhang, L., Tang, M., Liu, J., Liu, H., Yang, H., Fan, S. et al. (2020) Knockout of two BnaMAX1 homologs by CRISPR/Cas9-targeted mutagenesis improves plant architecture and increases yield in rapeseed (*Brassica napus* L.). *Plant Biotechnol. J.* **18**, 644–654.
- Zhong, J., He, W., Peng, Z., Zhang, H., Li, F. and Yao, J. (2020) A putative AGO protein, OsAGO17, positively regulates grain size and grain weight through OsmiR397b in rice. *Plant Biotechnol. J.* **18**, 916–928.

Supporting information

Additional supporting information may be found online in the Supporting Information section at the end of the article.

Figure S1 Effects of long-term low temperature (LTs) on the stem structure of *Brassica napus*.

Figure S2 Size distribution of known and novel miRNAs from cold-treated *Brassica napus* seedlings.

Figure S3 Heat map of differentially expressed miRNAs (DEMs) detected by sRNA-Seq.

Figure S4 MA and Volcano plot of differentially expressed genes (DEGs) from C18 and C6.

Figure S5 qRT-PCR verification of cold-responsive genes and randomly selected genes.

Figure S6 Kyoto Encyclopedia of Genes and Genomes (KEGG) and GOBP enrichment analysis of differentially expressed genes (DEGs).

Figure S7 Heat map of genes targeted by differentially expressed miRNAs (DEMs).

Figure S8 Structure and sequence comparison of *miR397a* from different plant species.

Figure S9 *Bna-miR397a* inhibits the expression of *BnaLAC* genes.

Figure S10 Lignin deposition and content in C18 and C6 lines under cold stress.

Figure S11 Expression analysis of lignin synthesis related genes.

Figure S12 Investigation of reactive oxygen species (ROS) related indexes.

Figure S13 Expression analysis of genes involved in reactive oxygen species (ROS) scavenging system.

Figure S14 Expression analysis of genes involved in CBF/dehydration-responsive element binding (DREB) pathways.

Figure S15 *miR397a-LAC2* confers freezing tolerance in *Arabidopsis*.

Table S1 List of miRNAs detected from the sRNA-Seq data.

Table S2 Clusters of differentially expressed miRNAs (DEMs) based on K-means analysis.

Table S3 Clusters of differentially expressed genes (DEGs) based on K-means analysis.

Table S4 The predicted target genes of differentially expressed miRNAs (DEMs).

Table S5 Clusters of DE-targets based on K-means analysis.

Table S6 The miRNA-target modules based on correlation analysis.

Table S7 Statistical analysis of lignin related determination.

Table S8 Differentially expressed genes (DEGs) detected by Kyoto Encyclopedia of Genes and Genomes (KEGG) and Gene Ontology (GO) enrichment analysis.

Table S9 Primers used in the study.